Investigation of the Physicochemical Properties and Selective Anti-Cancer Efficacy of in-Plasma Treated PBS Using an Exclusive Liquid-Submerged Plasma Jet

DOI: 10.1109/TRPMS.2025.3572863
Handle: http://hdl.handle.net/1942/48152

No. TRPMS-2025-0086.R1

`Investigation of the physicochemical properties and selective anti-cancer efficacy of in-plasma treated PBS using an exclusive liquid-submerged plasma jet

P. Shali, N. Caz, J. Van den Bosch, R. Ghobeira, S. Aliakbarshirazi, M. Narimisa, R. Morent, E. Wolfs, N. De Geyter

***Abstract*—Cancer remains a leading cause of mortality, emphasizing the need for innovative therapies. Plasma-treated liquids, containing reactive oxygen and nitrogen species, have demonstrated therapeutic potential. This study investigates the physicochemical properties and anti-cancer efficacy of phosphate-buffered saline (PBS) treated using a novel liquid-submerged plasma jet, which enhances interactions between plasma species and the liquid for a more uniform treatment. Operational parameters including voltage, gas flow, and treatment time, were optimized concurrently. Notably, the submerged configuration produced significantly higher H_2O_2 concentrations in PBS (up to 2000 µM) compared to the above-liquid plasma set-ups reported in literature. However, NO_2^- concentrations remained low (6-18 µM). Voltage variations influenced H_2O_2 production but had a minimal effect on NO_2^-, while gas flow rates did not impact their concentrations. PBS maintained a stable pH, demonstrating its effective buffering capacity. Stability tests showed H_2O_2 remained stable at 21°C, slightly increased at 4°C, and decreased at 37°C; nitrites were stable below 21°C but slightly decreased at 37°C. Plasma-treated PBS selectively reduced oral squamous cell carcinoma (OSCC) cell viability while sparing healthy keratinocytes (HaCaT), with H_2O_2 identified as the primary anti-cancer agent. These findings suggest that PBS plasma-treated using a new liquid-submerged set-up shows potential as selective OSCC therapy.**

***Index Terms*— hydrogen peroxide, liquid-submerged plasma jet, nitrite, oral squamous cell carcinoma, plasma-treated PBS.**

I. INTRODUCTION

CANCER remains the second leading cause of global mortality, with conventional treatments (tumorectomy, chemotherapy, radiotherapy) often having limited effectiveness and/or severe side effects [1] [2]. In recent years, non-thermal atmospheric pressure plasma (NTAPP) has emerged as a promising alternative therapy [3] [4]. NTAPP is a partially ionized gas involving a complex reactive environment containing electrons, ions, free radicals, neutral molecules, localized electric fields, and UV radiation. Devices like plasma jets and dielectric barrier discharges (DBDs) produce NTAPP using different working gases such as helium, argon, air, or gas mixtures. When plasma components (ions, electrons, atoms, and molecules) interact with surrounding air or liquids (e.g., N_2, O_2, H_2O), they generate reactive molecules beneficial for different medical purposes [5] [6] [7]. Research has actually demonstrated NTAPP's ability to kill various cancer cells, including melanoma, breast, colon, pancreatic, head and neck, and glioblastoma cells [1] [3] [8] [9] [10]. This effect is primarily driven by a plasma-derived chemical cocktail of reactive oxygen and nitrogen species (RONS) including H_2O_2, O_3, NO_2^- and NO_3^-. These species penetrate cancer cells, weaken antioxidant defenses, damage proteins and DNA, and activate apoptosis-related signaling pathways, ultimately leading to selective cancer cell death while minimizing harm to healthy cells [11] [12].

NTAPP-based cancer treatment can be applied directly or indirectly. In the direct treatment, tumors are exposed to plasma *in situ*, but safety concerns may arise due to body exposure to the electrical field, charged particles, and UV radiation [13]. Additionally, tissue conductivity and tumor irregularities can impact plasma homogeneity and RONS generation, leading to variable efficacy [14]. Direct treatment also requires specialized equipment and expertise to generate a fully controlled plasma effluent, which may not be widely available [15]. These challenges, combined with poor tissue penetration and difficulty in reaching deep organs, limit its effectiveness for non-superficial cancers and deep-seated tumors [14] [16].

P. Shali and N. De Geyter acknowledge the support of the Special Research Fund of Ghent University in financing the interdisciplinary project 01IO2018. M. Narimisa also acknowledges the support of the Special Research Fund of Ghent University in financing her postdoctoral position (01P06122). This work did not involve human subjects or animals in its research. (This work reflects the collaborative contributions of P. Shali, N. Caz, and J. Van den Bosch as co-first authors.) (E. Wolfs and N. De Geyter share joint last authorship.) (Corresponding author: Parisa Shali)

P. Shali, R. Ghobeira, S. Aliakbarshirazi, M. Narimisa, R. Morent, N. De Geyter are with the Research Unit Plasma Technology (RUPT), Department of Applied Physics, Faculty of Engineering and Architecture, Ghent University, Sint-Pietersnieuwstraat 41 B4, 9000 Ghent, Belgium (e-mail: Parisa.Shali@UGent.be; Rouba.Ghobeira@UGent.be; Sheida.Aliakbarshirazi@UGent.be; Mehrnoush.Narimisa@UGent.be; Rino.Morent@UGent.be; Nathalie.DeGeyter@UGent.be).

N. Caz, J. Van den Bosch, E. Wolfs are with Biomedical Research Institute (BIOMED), Laboratory for Functional Imaging and Research on Stem Cells (FIERCE Lab), Hasselt University, Agoralaan building C, 3590 Diepenbeek, Belgium (e-mail: nuran.caz@uhasselt.be; jolien.vandenbosch@uhasselt.be; esther.wolfs@uhasselt.be).

Color versions of one or more of the figures in this article are available online at http://ieeexplore.ieee.org

To overcome these challenges, indirect treatment was introduced as an elegant alternative. In this approach, a liquid is first treated with plasma and then applied to cancer cells or tissue. Plasma-treated liquids (PTLs) offer the advantage of being prepared in advance, functioning as a "drug" that can be used as an "off-the-shelf therapy" [3]. This allows for versatile administration methods, including topical application, localized perfusion, intraoperative irrigation, intraperitoneal cavity injection, or integration into biomaterials for sustained release near tumor sites, making PTLs a flexible and clinically relevant cancer treatment option [17] [18] [19] [20].

In the vast majority of studies utilizing PTLs for cancer treatment (> 95%), plasma was generated in the gas phase above the liquid to be treated (Supplementary Table 1). To the best of our knowledge, only two studies have reported the use of an in-liquid plasma jet to treat deionized water for cancer applications [21] [22].

Despite their widespread use, above-liquid plasma jets primarily interact with the liquid surface, leaving most of the volume largely unexposed. Consequently, research has demonstrated significant spatial and temporal inhomogeneity in RONS distribution within the liquid, with higher concentrations near the surface and delayed transport to deeper layers due to the limited penetration of plasma-generated species [23]. Chemical reactions or by-product formations at the surface may differ from those occurring in the bulk liquid. Additionally, short-lived reactive species that act as precursors for RONS formation may decay before diffusing into deeper regions, leading to suboptimal RONS concentrations. The efficiency of chemical activation in the treated liquid is also constrained by multiple factors. Plasma-generated species must traverse the ambient air before reaching the liquid interface and diffusing into the liquid bulk [24]. During this transit, many RONS undergo recombination or degradation, which can significantly reduce the flux of active species arriving at the liquid interface [25]. Alongside these limitations, the volume of the treated liquid plays a significant role in determining the concentration of generated reactive species. By reviewing species concentrations and treated volumes across various studies [26] [27] [28] [29] [30] [31] [32] [33], it can be concluded that increasing the treated volume (>2 mL), even with extended treatment times, results in significantly lower RONS concentrations. This reduction is attributed to a lower surface-area-to-volume ratio, which limits the plasma's ability to efficiently transfer reactive species into the liquid bulk [34][35]. In larger volumes, the accumulation of reactive species near the plasma-liquid interface, creates more pronounced concentration gradients with the liquid bulk remaining relatively unaffected.

Longer diffusion distances required for species to distribute throughout the liquid, coupled with enhanced recombination and quenching of short-lived radicals, further reduce their effective concentration [24]. Moreover, maintaining consistent RONS generation and concentration is challenging due to constant exposure to ambient air. Variations in humidity, temperature, and atmospheric composition influence plasma chemistry, affecting reproducibility.

To address these challenges, this paper proposes a newly designed atmospheric pressure plasma jet (APPJ) that is directly ignited in the liquid being treated. Unlike the above-liquid plasma configuration, this innovative set-up intensifies the interactions between plasma species and the liquid, significantly enhancing reactive oxygen species (ROS) generation, even in larger liquid volumes (>2 mL). By generating plasma within the aqueous phase, this configuration promotes a more homogeneous treatment, with reactive species evenly distributed throughout the liquid rather than concentrated at the surface. Short-lived radicals and metastable states remain near their generation sites, further boosting ROS levels. Most notably, this newly designed APPJ achieves substantially higher H_2O_2 concentrations in PTLs compared to conventional above-liquid plasma treatments, as well as the two existing studies using submerged plasma jets for cancer treatment [21] [22] [36] [26] [37] [38]. Moreover, this approach enhances treatment control and reproducibility, as the impact of ambient air is significantly minimized. This breakthrough configuration represents a major advancement in plasma-liquid applications, particularly for generating high H_2O_2 concentrations and treating larger liquid volumes with improved efficiency. These features underscore the set-up's relevance for scaling up indirect plasma treatments, especially when transitioning to complex three-dimensional tumor models or clinical scenarios, where both sufficient reactive species availability and larger liquid volumes are critical. As such, this new set-up stands out as a promising candidate for advancing plasma medicine toward translational and therapeutic use.

This high generation of H_2O_2 is particularly interesting in the context of cancer treatment due to its well-established role as a key mediator of PTL-induced cytotoxicity. While some studies suggest that H_2O_2 alone drives this effect, others emphasize the necessity of a synergistic interaction between H_2O_2 and NO_2^- to enhance anti-tumor activity [22] [37] [39]. Despite this, only a limited number of studies (approximately 30%, as shown in Supplementary Table 1) have directly compared PTLs to reconstituted liquids with matched concentrations of exogenous H_2O_2, NO_2^-, and/or their combination to verify whether the observed anti-tumor effects stem solely from these species or their synergy. Furthermore, such controls are crucial for evaluating whether PTLs generated using the novel submerged APPJ configuration exhibit higher cytotoxicity, suggesting that additional plasma-derived RONS contribute to their anticancer activity. Beyond efficacy, understanding PTL-induced effects is also crucial for evaluating their selectivity. While PTLs are reported to preferentially target cancer cells, less than half of the studies investigating their anti-cancer effects have included healthy cells for comparative analysis (as shown in Supplementary Table 1). Such comparisons are particularly crucial, as a few studies have indicated that PTLs may also exhibit non-selective cytotoxic effects [40] [6].

In view of the above, an exclusive APPJ operating in argon (Ar) is used in this work to treat phosphate-buffered saline (PBS) in its bulk. PBS is specifically selected because it mimics physiological conditions, maintaining pH balance, osmolarity, and ion concentrations similar to those in the human body [41]. The primary goal is to investigate the influence of key

operational parameters—such as voltage, gas flow rate, and treatment duration—on the plasma generation and on various physicochemical properties of the treated liquid. These properties include H_2O_2 and NO_2^- concentrations, pH, conductivity, temperature changes, and liquid loss following plasma treatment. Additionally, the stability of plasma-treated PBS is assessed by evaluating the aging effects during storage at 3 different temperatures (4°C, 21°C, and 37°C) over varying time periods. PTLs with optimal conditions and corresponding reconstituted H_2O_2 and/or NO_2^- controls are then used to treat human oral squamous cell carcinoma (OSCC) cells and healthy human keratinocytes (HaCaT cells) as an initial proof-of-concept of their selectivity. OSCC cells are purposely chosen because OSCC is an aggressive and prevalent form of neck and head cancer, particularly affecting the oral cavity. Despite all therapy advances, the 5-year survival rate of OSCC patients is still only around 50 %, and current treatments are associated with severe complications. Therefore, investigating PTLs as a promising alternative treatment is crucial, especially that in OSCC cells RONS levels are already elevated [42] [43] [44] [45].

Taken together, this is the first study to concurrently investigate a novel APPJ submerged in the treated liquid, analyze the impact of operational parameters on the liquid's physicochemical properties, assess effects on both healthy and cancer cells, and compare results with three chemically reconstituted controls.

II. Materials and Methods

A. Plasma treatment of PBS

A liquid-submerged APPJ was used to treat PBS. A schematic representation of the reactor composed of an aluminum pin serving as high-voltage electrode and a copper ring acting as the ground electrode is shown in Figure 1 (a). In short, the aluminum pin is tightly embedded in a cylindrical quartz tube having a length of 110.4 mm and inner and outer diameters of 1.1 and 3.1 mm respectively. The copper ring, with an inner and outer diameter of 3.1 mm and 13 mm respectively, and a height of 10.5 mm, was fixed in a Teflon shell in a way that it surrounds the quartz tube. The distance between the grounded ring and the tip of the high-voltage pin electrode was set at 18 mm. The high-voltage pin electrode was connected to a 50 kHz sinusoidal custom-made power supply exhibiting a maximum output voltage of 25 kV peak-to-peak.

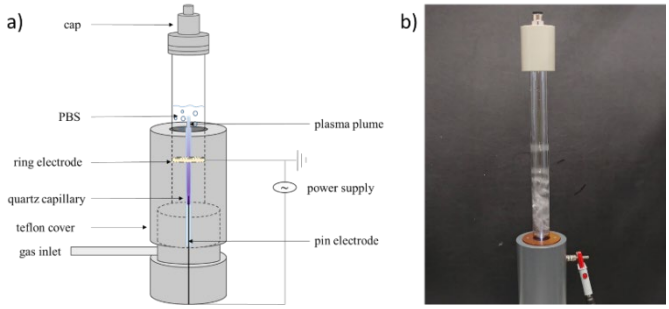

Figure 1. Schematic representation (a) and photograph (b) of the APPJ submerged in PBS.

To perform the plasma treatment, argon (Alphagaz 1, Air Liquide, Belgium) was used as carrier gas. The gas was fed into the quartz tube at pre-determined flow rates controlled by a mass flow controller (Model F-201CV, Bronkhorst, The Netherlands). Thereafter, 5 mL of PBS (Carl Roth GmbH, Germany) was poured into a tubular glass sample holder (inner and outer diameter of 16.5 mm and 22.5 mm respectively) that was perforated at its bottom to slide around and to enclose the end of the quartz capillary. This set-up enabled the plasma jet to extend into the bulk of the PBS when a sufficiently high voltage is applied. The variable process parameters were the plasma exposure time (1–10 min), the gas flow rate (1–2.5 standard liters per min (slm)), and the voltage (2–3.5 kV). The ranges for the voltage and gas flow rate were determined based on operational constraints. Applying a voltage of more than 3.5 kV increased the electrical discharge activity, which destabilized the plasma jet and caused overheating, potentially damaging the plasma generating equipment during extended treatment times. Furthermore, gas flow rates above 2.5 slm could also not be used, as the very high gas velocity resulted in the ejection of PBS out of the sample holder, compromising experimental reproducibility and accuracy. In each experiment, one single operational parameter was varied while the other parameters remained unchanged. An overview of the different plasma operational conditions can be found in Table 1.

For the liquid aging analysis, samples were exposed to plasma for 10 minutes using a fixed voltage of 3 kV and a gas flow rate of 2 slm. After plasma treatment, samples were stored for periods of 7, 14, and 21 days at various temperatures (4, 21, and 37 °C) to assess the effects of storage temperature on the stability of plasma-treated PBS.

Table 1. Summary of the used experimental conditions, showing the variable and fixed parameters during PBS plasma treatment.

Experimental conditions		Values		
Varying parameter	Fixed parameters	Voltage	Flow rate	Treatment time
Voltage	Flow rate and treatment time	2 – 3.5 kV	2.0 slm	10 min
Flow rate	Voltage and treatment time	3.0 kV	1 – 2.5 slm	10 min
Treatment time	Voltage and flow rate	3.0 kV	2.0 slm	1 – 10 min

B. Electrical and optical characterization of the APPJ

The discharge power of the APPJ was assessed at different voltages and flow rates via the analysis of corresponding voltage-current waveforms. To do so, a high-voltage probe (P6015A, Tektronix) was connected to the pin electrode. The discharge current was acquired by measuring the voltage over a non-inductive resistor (100 Ω) positioned in series with the APPJ. The ensuing voltage-current waveforms were then recorded by a PC oscilloscope (PicoScope 3204A) and used to calculate the discharge power.

The anti-cancer properties of PTLs most likely rely on the generation of specific RONS originating from, amongst others, excited plasma species. Therefore, the presence of these excited radiative species was assessed in the Ar APPJ using optical characterization. To do so, optical emission spectroscopy (OES) measurements were performed using a quartz optic fiber (FC-UVIR600-2, Avantes, The Netherlands) with a collimating lens (COL-UV/VIS, Avantes, The Netherlands) connected to an S2000 spectrometer (Ocean Optics Inc., USA). During the experiment, the optic fiber was positioned perpendicular to the capillary tube at the beginning of the plasma plume, and approximately 10 mm away from the glass sample holder. This configuration ensured an optimal collection of the emitted light for spectroscopic analysis. The exposure time was set to 700 milliseconds, which is a duration that could adequately capture spectral emissions. Additionally, to further enhance the accuracy and reliability of the collected data, the OES spectra were averaged over 7 measurements per condition. These spectra were acquired in a wavelength range of 200-900 nm with a resolution of 0.3 nm.

C. Hydrogen peroxide quantification in PBS

To quantify the concentration of H_2O_2 in plasma-treated PBS, a titanium oxysulfate assay was employed. This assay relies on the reaction between H_2O_2 and Ti_4^+ ions, resulting in the formation of pertitanic acid, which exhibits a yellow color with maximum absorption at approximately 407 nm [37]. To prevent degradation of the formed H_2O_2 by NO_2^-, sodium azide (NaN_3) was used as a nitrite scavenger. Directly after the plasma treatment, 15 µL of NaN_3 (Carl Roth GmbH, Germany) was added to 400 µL of PBS, followed by the addition of 200 µL of $TiOSO_4$ (purity ≥29% Ti, Sigma-Aldrich, Belgium) dissolved in 2 M sulfuric acid (98%, Rotipuran, Carl Roth, Germany) reagent. The mixture was then incubated in the dark for 20 min. Subsequently, the absorbance of the resulting solution was measured using a UV Mini-1240 spectrophotometer (Shimadzu Co., Japan). To ensure accurate measurements, a similar mixture of untreated PBS with added NaN_3 and $TiOSO_4$ was used as a baseline, thereby eliminating any overestimation in the concentration of the plasma-induced H_2O_2. The H_2O_2 concentration was then determined using a calibration curve that was constructed based on known standards. The reported values represent the average concentrations and standard deviations calculated based on 4 measurements conducted on 4 separately plasma-treated PBS samples for each experimental condition.

D. Nitrite quantification in PBS

To determine the concentration of nitrite in plasma-treated PBS, the Griess assay was employed [46]. In fact, when the Griess reagent, consisting of sulfanilamide and N-(1-naphthyl)ethylenediamine, is added to the treated PBS, the present nitrite ions will react with sulfanilamide forming a diazonium salt. This salt will then react with N-(1-naphthyl)ethylenediamine generating a red-pink azo dye that exhibits a maximum absorption at approximately 540 nm. For these reactions to occur, 400 µL of the Griess reagent was added, directly after the plasma treatment, to 400 µL of PBS. The Griess reagent solutions were prepared by mixing 1 g of sulfanilic acid (Merck, Germany) and 0.1 g of N-(1-naphthyl)ethylenediamine (purity ≥98%, Sigma-Aldrich, Belgium) with 2.3 mL of phosphoric acid (85%, also obtained from Sigma-Aldrich, Belgium). Subsequently, the mixture was incubated in the dark for 10 min. The absorbance of the resulting solution was measured using a UV Mini-1240 spectrophotometer (Shimadzu Co., Japan). As a baseline reference, an untreated sample-Griess reagent mixture was used. Based on known standards, a calibration curve was constructed to determine the concentration of NO_2^-. The reported values represent the average concentrations and standard deviations calculated based on 4 measurements conducted on 4 separately plasma-treated PBS samples for each experimental condition.

E. Nitrate quantification in PBS

Nitrite concentration in treated PBS was measured using the salicylic acid nitration method [47]. Briefly, 250 µL of each sample was mixed with 800 µL of a 5% (w/v) salicylic acid (Sigma Aldrich, Belgium) solution prepared in 98% sulfuric acid (Rotipuran, Carl Roth, Germany). The mixture was incubated at room temperature until cooled, after which 10 mL of an 8% (w/v) NaOH (Carl Roth GmbH, Germany) solution was added. Once the solution returned to room temperature, its absorbance was recorded at 410 nm using a Shimadzu UV Mini-1240 spectrophotometer (Shimadzu Co., Japan). An untreated PBS sample combined with reagent served as the baseline reference, and a calibration curve based on known standards was used to calculate nitrate concentrations.

F. *pH of PBS pre- and post-plasma treatment*

pH of untreated and plasma-treated PBS were measured using a FiveEasy Plus™ pH meter FE20 (Mettler Toledo, Switzerland). The pH meter was equipped with a pH combination electrode InLab® VersatilePro. All measurements were done 4 times using 4 independently prepared plasma-treated samples for each condition.

G. Cell culture

Human OSCC cells (UM-SCC-14C line; obtained from CLS cell lines service) were cultured in Dulbecco's Modified Eagle Medium/Nutrient Mixture F-12 (Gibco™, Thermo Fisher Scientific), supplemented with 5% fetal bovine serum (FBS) and 1% penicillin/streptomycin. Human HaCaT cells (obtained from CLS cell lines service) were cultured in Dulbecco's Modified Eagle Medium (Gibco™, Thermo Fisher Scientific), supplemented with 10% FBS and 1% penicillin/streptomycin. Both cell lines were incubated at 37°C with 5% CO_2. Medium was replaced 3 times per week and cells were passaged once a week at a density of 1/10. Each cell type was maintained in its respective optimized medium to preserve its characteristic metabolic and physiological properties, as using a single medium for both could introduce additional stress and confound results.

H. Cell proliferation and viability assays

Cells were seeded at a density of $15x10^3$ cells/cm^3 and allowed for overnight adherence. Subsequently, the different PBS-treated conditions were added to the cells in a 1/5 dilution in culture medium. The different conditions include: untreated PBS, plasma-treated PBS (3-minute treatment, 2 slm gas flow, 3 kV voltage), PBS exposed to the Ar gas flow without plasma ignition, and PBS supplemented with concentrations of exogenous H_2O_2, NO_2^-, and H_2O_2 + NO_2^- matching those of the plasma-treated PBS. These controls were included to assess the individual effects of gas flow, plasma treatment, H_2O_2, NO_2^-, and their combination.

Following treatment, cells were imaged every 2 hours for a duration of 72 hours at 10x magnification using the Incucyte S3® Live-Cell Analyzer (Sartorius, Germany). Confluency was analyzed using the Incucyte software to study cell proliferation. For cell viability assessment, the cells were incubated with AlamarBlue (Bio-Rad, USA) according to the manufacturer's instructions 24, 48 and 72 hours after treatment. Fluorescence intensity was measured at 530/590 nm wavelength using the CLARIOstar PLUS plate reader (BMG Labtech, Germany), and data were normalized alccording to the untreated PBS control (negative control). Each experiment was performed in triplicate and repeated 3 times to ensure accuracy.

I. Statistical analysis

All statistical analyses were performed using GraphPad Prism 9. The cell viability experiments were analyzed using the Two-way ANOVA with Šídák's multiple comparisons test. For the proliferation tests, the mixed-effect analysis followed by Dunnett's multiple comparisons was used.

III. Results and discussion

A. Electrical characterization of the APPJ

The electrical characteristics and operational mode of the liquid-submerged APPJ were evaluated to fine-tune the plasma treatment procedure. To evaluate the Ar discharge mode and determine the mean discharge power, voltage-current (V-I) waveforms were plotted. Argon was chosen as the discharge gas due to its ability to produce a stable glow-like plasma at relatively low gas temperatures [48]. Supplementary Figure 1 illustrates the V-I waveforms of the Ar APPJ generated at an applied voltage of 3.0 kV and a gas flow rate of 2.0 slm, supporting this choice.

To calculate the discharge power at different process parameters (gas flow rate and applied voltage), the following equation was used:

$$P = \frac{1}{T}\int I(t)V(t)dt \qquad Eq\ 1$$

Where T represents the period of the voltage, while I and V denote the discharge current and voltage, respectively.

Figure 2 (a) shows a clear increase in discharge power with increasing voltage, which is expected based on the power calculation formula (*Eq 1*). At 2.0 kV, the discharge power is 3.0 ± 0.6 W, while at 3 kV, it increases to 5.2 ± 0.1 W. This increase in power can be attributed to the stronger electric field within the discharge as the voltage increases, which enhances ionization levels and results in more intense plasma generation [49]. Consequently, more electrical energy is required to sustain the discharge leading to a rise in the discharge power. In contrast, an increase in gas flow rate has little impact on the discharge power, as shown in Figure 2 (b). At a gas flow rate of 1.0 slm, the power is 4.2 ± 0.3 W, and as the flow rate increases, this value remains within the error margin, reaching 4.4 ± 0.2 W at 2.5 slm. These findings align with previous studies on plasma jets, which also report that the flow rate has minimal influence on the discharge power, unlike the more pronounced effect of applied voltage [50] [51].

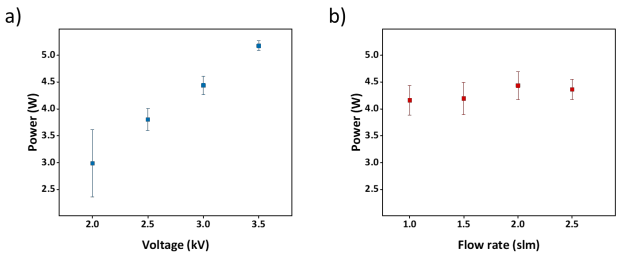

Figure 2. Discharge power measured via the V-I method as a function of voltage (a) and gas flow rate (b).

B. Optical emission spectroscopy results

Basic optical diagnostics of the submerged Ar APPJ in PBS were performed by means of OES to gain insights into plasma-liquid interactions. These measurements allow the identification of radiatively excited species, helping to pinpoint the potential contributors to the generation of RONS, specifically H_2O_2 and NO_2^-. The OES spectrum shown in Figure 3 corresponds to the Ar APPJ ignited with a flow rate of 2 slm and an applied voltage of 3 kV. This spectrum is dominated by intense Ar I emission lines (Ar(4p → 4s)) at 696.5 nm ($2p_2$ to $1s_5$), 706.7 nm ($2p_3$ to $1s_5$), 727.3 nm ($2p_2$ to $1s_4$), 738.4 nm ($2p_3$ to $1s_4$), 750.4 nm ($2p_1$ to $1s_2$), 763.5 nm ($2p_6$ to $1s_5$), 772.4 nm ($2p_2$ to $1s_3$), 794.8 nm ($2p_4$ to $1s_3$), 801.5 nm ($2p_8$ to $1s_5$), 811.5 nm ($2p_9$ to $1s_5$), 826.5 nm ($2p_2$ to $1s_2$), 842.5 nm ($2p_8$ to $1s_4$) and 852.1 nm ($2p_4$ to $1s_2$). This trend was also observed in several previous studies in which Ar discharges were optically characterized [52] [53] [54]. The excited Ar species are generated as follows [55]:

$$Ar + e \rightarrow Ar^* + e \quad (1)$$

Next to the present Ar emission lines, the recorded spectrum displays emission bands from nitrogen, specifically the N_2 second positive system, due to the N_2 ($C^3\Pi_u - B^3\Pi_g$) transition. These appear at wavelengths 315.8 nm, 337.2 nm, 357.8 nm, 375.2 nm, 380.4 nm, 405.0 nm, 415.9 nm, 420.1 nm, 425.9 nm and 434.4 nm [56] [57] [58] [59]. Moreover, weak intensity lines linked to the N_2^+ first negative system, corresponding to the $B^2\Sigma_u^+$-$X^2\Sigma_g^+$ transition, are perceived at 391.4 nm [56] [60] [61]. The presence of these N_2 and N_2^+ systems likely originate from ambient air diffusing into the PBS, which interacts with the plasma jet afterglow. These excited nitrogen states are generated via numerous reactions, such as pooling reactions, electron impact processes of the ground state N_2 ($X^1\Sigma_g^+$), and transfer of energy as a result of inter-particle collisions and association excitations [62]. For instance, the N_2 ($C^3\Pi_u$) state could be generated by electron impact excitation of the N_2 ground state or via excited Ar species, as shown in reactions (2) and (3), respectively [52] [55] [62]:

$$N_2 (X^1\Sigma_g^+) + e \rightarrow N_2 (C^3\Pi_u) + e \quad (2)$$
$$N_2 (X^1\Sigma_g^+) + Ar^* \rightarrow N_2 (C^3\Pi_u) + Ar \quad (3)$$

The N_2^+ ($B^2\Sigma_u^+$) state may be formed via electron impact ionization, as illustrated in reaction (4), or via collision with highly vibrational N_2 molecules ($X^1\Sigma_g^+$), as depicted in reaction (5) [62] [63]:

$$N_2 (X^1\Sigma_g^+) + e \rightarrow N_2^+ (B^2\Sigma_u^+) + 2e \quad (4)$$
$$N_2 (X^1\Sigma_g^+)_{v \geq 12} + N_2^+ (X_2\Sigma_g^+) \rightarrow N_2^+ (B^2\Sigma_u^+) + N_2 (X^1\Sigma_g^+)_{v-12} \quad (5)$$

In Figure 3, a relatively high intensity peak corresponding to hydroxyl radicals (˙OH) is detected at a wavelength of 309.9 nm [64]. This ˙OH, due to the transition $A^2\Sigma^+$-$X^2\Pi$, most likely originates from reactions between H_2O molecules present in PBS and electrons or excited Ar atoms, as illustrated in reactions (6) and (7), respectively [55] [58]:

$$H_2O + e + \Delta E \rightarrow {}^{\cdot}OH (A^2\Sigma^+) + H + e \quad (6)$$
$$H_2O + Ar^* \rightarrow {}^{\cdot}OH (A^2\Sigma^+) + H + Ar \quad (7)$$

Finally, another peak at 777.7 nm corresponds to atomic oxygen O I ($3p^5P$ to $3s^5S$), which can be generated either by dissociative collisions of O_2 molecules (in the provenance of the surrounding air) or by electrons Penning ionization between O_2 molecules and excited Ar, as shown in reactions (8) and (9), respectively [37] [62]:

$$O_2 + e \rightarrow 2O + e \quad (8)$$
$$Ar^* + O_2 \rightarrow 2O + Ar \quad (9)$$

Importantly, unlike in typical OES spectra recorded for plasma jets above liquids, where the environment surrounding the plasma plume is rich in nitrogen [65] [66] [67], no NO_γ emission (200-280 nm) was detected. Additionally, no emission lines corresponding to atomic nitrogen were perceived, most likely due to the plasma being ignited within the liquid rather than in ambient air, where nitrogen molecules are more prevalent. Furthermore, the lower dissociation energy of oxygen compared to nitrogen further supports this observation, as the presence of oxygen may suppress atomic nitrogen [68].

The two studies conducted by Chen et al. [21] [22] on liquid treatment using a liquid-submerged plasma set-up support the OES findings of this study, despite detecting additional peaks corresponding to N_2 and N_2^+, along with weak NO emission lines in the 250–300 nm range. This is likely due to the use of industrial-grade Ar probably containing nitrogen impurities as the feed gas.

Finally, it is important to mention that OES spectra as a function of the applied voltage and gas flow rate are not included in this study as averaging the emitted light over the entire line of sight masks critical spatial variations in plasma properties such as temperature, density, and composition. This masking effect hinders the accurate interpretation of localized changes and the dynamics of reactive species [69].

To conclude, the OES spectra of the submerged Ar APPJ indicate the presence of excited Ar atoms, excited N_2 and N_2^+ molecules, excited ˙OH radicals, and excited oxygen atoms in the plasma effluent.

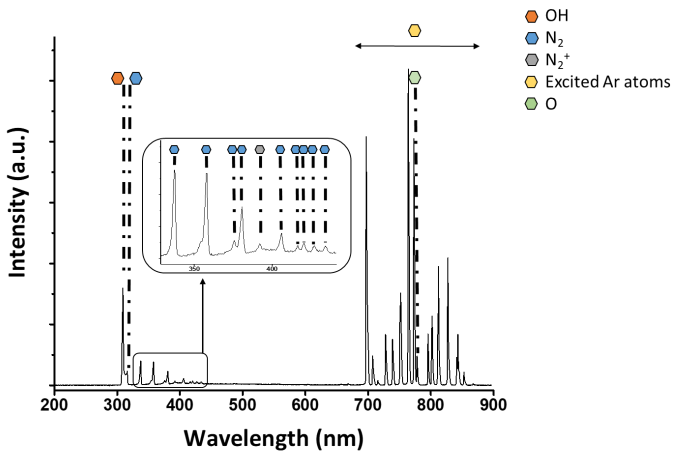

Figure 3. Optical emission spectrum of the Ar plasma ignited in the PBS bulk (gas flow rate: 2.0 slm; voltage: 3.0 kV).

C. Hydrogen peroxide concentration

The exposure of aqueous liquids to plasma discharges is known to generate significant amounts of hydrogen peroxide (H_2O_2) [70] [71] [72]. H_2O_2 can be generated in the liquid phase through the reaction between 2 hydroxyl radicals or between hydrogen and hydroperoxyl radicals, as shown below [73] [74]:

$$H_2O + e \rightarrow {}^{\cdot}OH + {}^{\cdot}H + e \quad (10)$$
$${}^{\cdot}OH + {}^{\cdot}OH \rightarrow H_2O_2 \quad (11)$$
$${}^{\cdot}H + O_2 \rightarrow HO_2{}^{\cdot} \quad (12)$$
$$HO_2{}^{\cdot} + {}^{\cdot}H \rightarrow H_2O_2 \quad (13)$$

In reaction (11), H_2O_2 can also form in the gas phase and subsequently dissolve into the liquid. In the set-up used in this study, PBS evaporation (discussed previously) increases the amount of water vapor, which elevates the levels of gaseous •OH radicals, as confirmed by OES and shown in reactions (6) and (7). These •OH radicals then form gaseous H_2O_2 via reaction (11), which dissolves into the liquid due to its high solubility (Henry's law constant: 1.92×10^6) [75], further increasing the H_2O_2 concentration [76].

As there is compelling evidence that plasma-induced H_2O_2 plays a major role in the cellular toxicity of plasma-treated liquids [77] [78] [79] [80] [81], it is essential to quantify the concentration of H_2O_2 generated in PBS. Figure 4 (a – c) shows the evolution of the H_2O_2 concentration as a function of voltage (a), flow rate (b), and treatment time (c).

Figure 4 (a) illustrates that the concentration of H_2O_2 increases from approximately 1500 µM at 2.0 kV to nearly 2000 µM at 3.5 kV. This increase is linked to the higher plasma power at increased voltages, as shown in Figure 2 (a). The rise in plasma power enhances electron density, promoting the dissociation of water molecules into •OH radicals, thereby boosting H_2O_2 production [82].

Figure 4 (b) reveals that the gas flow rate does not have a significant impact on the H_2O_2 concentration, consistent with Dimitrakellis *et al.* [83], who also observed minimal impact of gas flow rate on H_2O_2 production. This can be attributed to a rather stable discharge power across varying flow rates, as shown in Figure 2 (b).

Figure 4 (c) illustrates a linear increase in H_2O_2 concentration with plasma exposure time (R^2 = 0.99). After 10 minutes of plasma exposure, H_2O_2 levels reach 1750 µM, which is 3.64 times higher than after 1 minute (480.2 µM). The observed linear increase aligns well with previously published findings, as the linear temporal evolution of the H_2O_2 concentration in plasma-treated liquids has been noted in numerous studies [27] [70] [84] [85]. With increased treatment time, the dissociation of water molecules becomes more pronounced due to the longer contact time between the plasma species and the water molecules. This prolonged interaction leads to the production of higher amounts of H_2O_2 in the plasma-treated PBS. Moreover, the continuous generation of ROS in the liquid over time can maintain a reactive environment that gradually increases H_2O_2. The cumulative effect of these ongoing reactions results in an increase in H_2O_2 levels with prolonged exposure.

The data presented in Figure 4 (a) – (c) demonstrate that the advanced liquid-submerged plasma set-up configuration used in this work yielded very high H_2O_2 concentrations, reaching almost 2000 µM.

Table 2 compares the production of H_2O_2 across different set-ups and liquids in the current literature, with concentrations ranging from only a few µM up to 1320 µM [11] [14] [21] [84] [85] [86] [87] [88]. The studies were chosen for their diverse plasma configurations, carrier gases, operational parameters, and their significant findings on RONS production, providing a relevant benchmark to demonstrate the efficiency of the submerged plasma jet set-up used in this research. H_2O_2 concentrations attained in this study significantly surpass these values, demonstrating the superior efficiency of our submerged plasma configuration in generating H_2O_2.

Submerging the plasma directly in the liquid intensifies the interaction between plasma-generated species and the liquid, more efficiently generating long-living ROS species. This intense contact facilitates the transfer of energy and plasma species from the plasma to the liquid, enhancing the chemical reactions occurring into the liquid. When plasma is generated above the liquid, the reactive plasma species must travel over a certain distance before reaching the liquid surface. During their traveling, these species may recombine or interact with other molecules present in the air, thereby reducing their chemical reactivity by the time they reach the liquid [89]. Consequently, it has been observed that shorter distances between the plasma generation region and the liquid lead to increased ROS production in the liquid [37] [89] [90]. In this study, the direct generation of plasma in the liquid, confines the reactive plasma species within the liquid medium, limiting their recombination, and preserving their chemical reactivity, which in turn results in an enhanced H_2O_2 production.

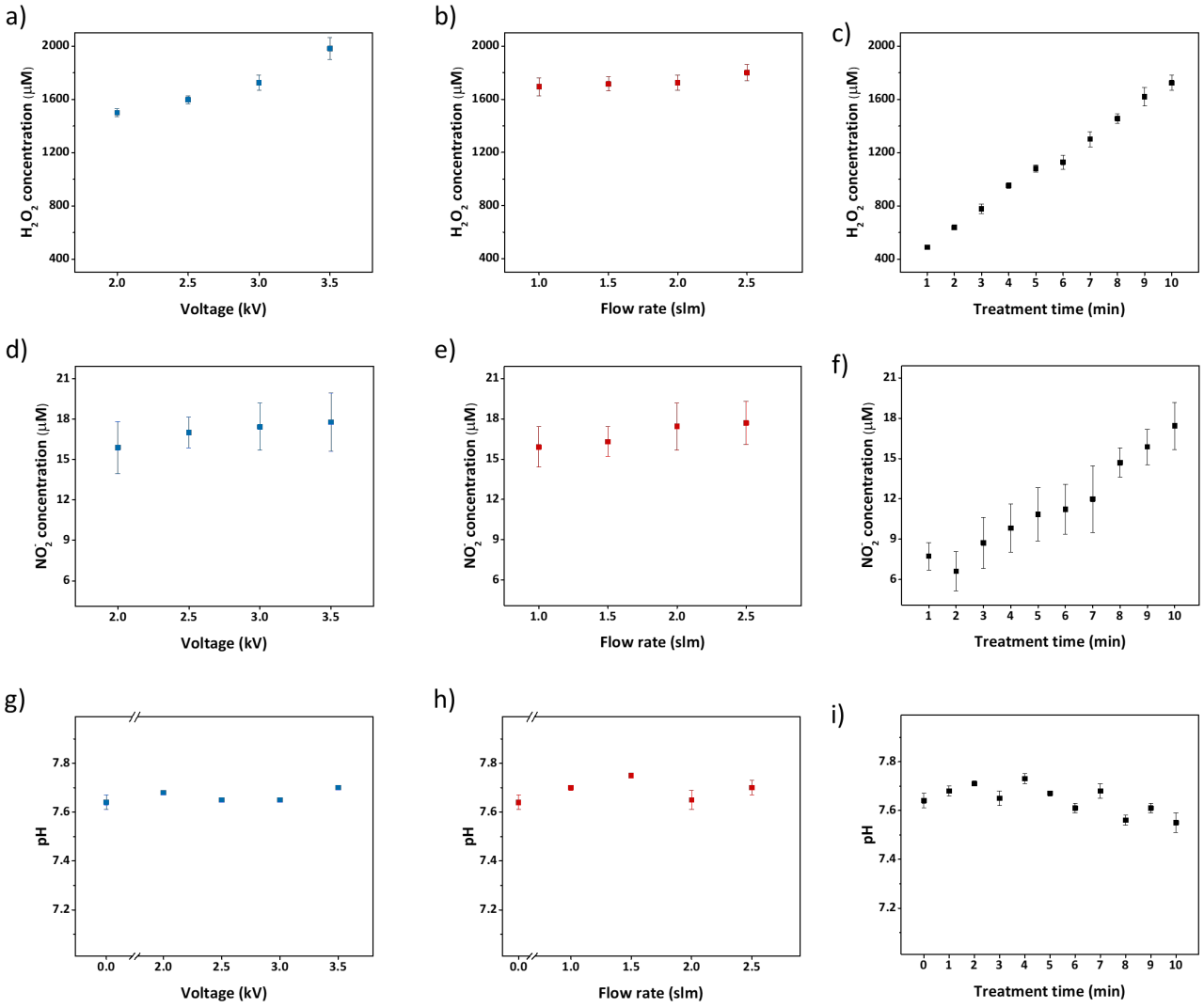

Figure 4. (a) Evolution of the H_2O_2 concentration of PBS exposed to plasma as a function of voltage, (b) flow rate, and (c) treatment time. (d) NO_2^- concentration in plasma-treated PBS as a function of voltage, (e) flow rate, and (f) treatment times up to 10 minutes. (g) pH of plasma-treated PBS as a function of voltage, (h) flow rate, and (i) plasma treatment time.

As illustrated in Table 2, Chen *et al.* [22] compared H_2O_2 production in submerged versus above-liquid plasma configurations and found that the submerged set-up produces higher H_2O_2 concentrations. However, the plasma set-up used in this study achieves significantly higher H_2O_2 levels compared to the work of Chen *et al.* and another study that also used a plasma submerged in liquid [21] [22]. Several factors influence the generation of ROS species, including the carrier gas, discharge power, distance between electrodes, electrode geometry, power supply characteristics, and the type of liquid [91] [92] [93]. The unique design of our set-up, which allows for efficient plasma-liquid interaction, contributes to the enhanced H_2O_2 production observed in this study, outperforming other submerged plasma systems. This is particularly significant because H_2O_2 is a key reactive species responsible for inducing oxidative stress and apoptosis in cancer cells [94] [95]. Notably, this new system does not only address the challenge of generating high H_2O_2 concentrations but also achieves this in larger volumes, highlighting its potential for scaling up indirect plasma treatments. This is especially important for more complex tumor models and clinical applications, where both high H_2O_2 levels and larger volumes are critical. However, while the superior H_2O_2 yield highlights a strength of our system, it is important to acknowledge that this comes with relatively limited production of NO_2^- (as detailed in the following section). In fact, although H_2O_2 is frequently cited as the primary driver of PTL-mediated cytotoxicity, mounting evidence points to a synergistic role for NO_2^- in enhancing anti-tumor effects [96]. Specifically, the interaction between H_2O_2 and NO_2^- has been shown to lower the cytotoxic threshold for malignant cells without increasing toxicity toward healthy cells [78]. This observation does not diminish the significance of our findings but rather underscores that, while achieving high H_2O_2 concentrations in scalable volumes represents a substantial advancement, it should not be regarded as the only reactive species of importance in plasma-based therapies.

Table 2: Efficiency of different plasma set-ups using different liquids, carrier gases, and operational parameters in the generation of H_2O_2, NO_2^-, and NO_3^- as detected in the current literature. CAP stands for cold atmospheric plasma. The values marked with a single asterisk (*) indicate the concentrations of H_2O_2, NO_2^-, and NO_3^- as reported in the original studies cited in the table. The values marked with a double asterisk (**) represent the concentrations observed in the current study at a plasma treatment time comparable to that used in the cited study.

Plasma set-up	Liquid	Gas	Distance to the liquid surface (mm)	Liquid volume (mL)	H_2O_2 (µM)		NO_2^- (µM)		NO_3^- (µM)		Treatment time (min)	Ref.
					*	**	*	**	*	**		
Piezoelectric direct discharge plasma	Saline	Air	0.5	5	15.7	638.4	90	6.61	870.7	0	2	[86]
Plasma pen	PBS	Ambient air	10	5	123.6	1727	118.8	17.43	48.9	0	10	[97]
µCAP	Deionized water	He	3	0.1	26.1	638.4	133.1	6.61	-	0	2	[88]
DBD	PBS	Ambient air	42	0.15	79.4	1082	3580	10.84	3045	0	5	[98]
Plasma jet	PBS	He	20	0.1	680	638.4	360	6.61	315	0	2	[38]
	NaCl 0.9%				515		160		180	0		
	PBS	Ar	10	2	1320.6	1621.2	481.1	15.87	-	0	9	[37]
			15		358.3		253.3		-	0		
			30		188.6		186.8		-	0		
	Saline	Ar	8	3.35 (for NO_2^- and NO_3^-), 3.8 (for H_2O_2)	600	1727	10	17.43	101	0	10 min/mL	[26]
	Distilled water	Air	42	10	100	-	1200	-	1100	-	20	[36]
	PBS				191		3320		844	-		
	Deionized water	Ar	Not mentioned	200	2.9	-	4.4	-	-	-	30	[22]
		He			0.2		1.3		-	-		
		N_2			0.02		0.2		-	-		
	Deionized water	Ar	Submerged in liquid	200	8.1	-	18.1	-	-	-	30	[22]
		He			6.9		17.4		-	-		
		N_2			2.7		3.9		-	-		
	Deionized water	He	Submerged in liquid	-	13	-	4	-	-	-	30	[21]
kINPen IND device	Alginate solution	Ar	10	1	941	1727	177	17.43	321	0	10	[99]

D. Nitrite concentration

In addition to H_2O_2, the presence of reactive nitrogen species such as nitrates (NO_3^-) and nitrites (NO_2^-) in PTLs is crucial due to their significant biological effects, including their anti-cancer properties [84] [100] [101]. Hence, this study focused on the detection of NO_3^- and NO_2^- ions in plasma-treated PBS. However, under the experimental conditions used in this work, nitrates were not detected in the plasma-treated PBS, indicating that the submerged plasma jet used in this study does not produce these species. The absence of nitrate production can be attributed to the neutral pH of PBS, which inhibits the disproportionation of nitrites into nitrates and nitric oxide. Furthermore, the limited availability of oxygen restricts the oxidation of nitrite to nitrate [102]. Conversely, nitrite was detected in the plasma-treated PBS. Nitrite formation begins in the gas phase through the production of atomic nitrogen by two

primary pathways: chemical quenching of metastable argon by N_2 and electron impact dissociation of N_2 [103] [104]:

$$N_2 + Ar^* \rightarrow 2^{\cdot}N + Ar \quad (14)$$
$$N_2 + e \rightarrow 2^{\cdot}N + e \quad (15)$$

Subsequently, these nitrogen atoms react with molecular oxygen or •OH radicals to form nitric oxide ($^{\cdot}NO$) through the following reactions [103]:

$$^{\cdot}N + O_2 \rightarrow {}^{\cdot}NO + {}^{\cdot}O \quad (16)$$
$$^{\cdot}N + {}^{\cdot}OH \rightarrow {}^{\cdot}NO + {}^{\cdot}H \quad (17)$$

The presence of atomic oxygen and •OH radicals was also confirmed by OES. Furthermore, the interaction of plasma with N_2 from the air above the liquid resulting in the generation of excited nitrogen species, as observed by OES, indicates that nitric oxide formation can also be achieved [105]:

$$N_2^* + {}^{\cdot}O \rightarrow {}^{\cdot}NO + N^* \quad (18)$$
$$N^* + O_2 \rightarrow {}^{\cdot}NO + {}^{\cdot}O \quad (19)$$

Detecting the spectral lines of atomic nitrogen in the afterglow using OES is challenging due to their high reactivity and relatively weak transitions compared to the dominant peaks of molecular nitrogen [106]. Additionally, a prominent emission line from atomic nitrogen has been previously identified at 120 nm [107]. Nonetheless, this wavelength falls outside the wavelength range utilized in this study, which begins at 200 nm. Consequently, while the N peak may not be visible in the OES data, atomic nitrogen may still be present, albeit in very low concentrations.

It is also worth mentioning that the generation of excited •NO is initiated by electron impact excitation of ground-state •NO, an additional step that likely accounts for the absence of NO* in the OES data. This detection challenge is compounded by the significantly shorter estimated lifetime of excited NO, which is approximately 2.5 times shorter than that of excited N_2 species [108].

The created •NO can undergo further oxidation to form $^{\cdot}NO_2$ [103]:

$$^{\cdot}NO + {}^{\cdot}O \rightarrow {}^{\cdot}NO_2 \quad (20)$$

Finally, $^{\cdot}$•NO and $^{\cdot}$•NO_2 generated in the gas phase readily dissolve in the liquid, leading to the formation of nitrites through the following reactions [103] [109] [110] [111] [112]:

$$NO_2 + NO + H_2O \rightarrow 2H^+ + 2NO_2^- \quad (21)$$
$$4^{\cdot}NO + O_2 + 2H_2O \rightarrow 4NO_2^- + 4H^+ \quad (22)$$
$$^{\cdot}OH + {}^{\cdot}NO \rightarrow HNO_2 \quad (23)$$

Figure 4 (d) and (e) show the effect of voltage and gas flow rate on nitrite production. Unlike the trend observed for H_2O_2, where higher voltages increased production, neither voltage nor gas flow rate significantly impacted nitrite levels. This discrepancy can arise from the fact that the nitrite formation relies on plasma interaction with atmospheric nitrogen above the liquid. Reactive species formed in the plasma may undergo multiple reactions as they travel from the nozzle to the liquid surface, including quenching by other molecules, dissolution into the liquid, or de-excitation through collisions. In the submerged configuration, the liquid acts as a barrier, reducing the availability of reactive species reaching the liquid surface and necessary for nitrite formation. Although higher voltages generate more plasma species, their efficiency in producing nitrites is limited by the insulating effect of the liquid. Instead, the energy boost primarily enhances the formation of reactive oxygen species due to the direct contact with the oxygen-containing liquid.

Similarly, variations in gas flow rate do not significantly change the nitrite concentration. Higher gas flow velocity increases the likelihood of quenching reactions, reducing the availability of reactive nitrogen species necessary for nitrite formation, which explains the minimal effect of this parameter on nitrite production.

Figure 4 (f) presents the impact of plasma treatment time on nitrite formation. Nitrite concentration increased from 7.73 µM after 1 minute to 17.43 µM after 10 minutes of plasma treatment, displaying a linear correlation (R^2=0.95) between treatment duration and nitrite production, similar to H_2O_2. This aligns with previous studies, published by Girard *et al.* and Sersenová *et al.*, who also observed a time-dependent increase in nitrite concentration in PBS exposed to plasma [6] [32]. The continuous production of RNS during prolonged plasma exposure leads to the accumulation of nitrites in the liquid. As detailed in chemical reactions (16-23), nitrogen in the gas phase reacts with electrons, oxygen, and water forming various nitrogen oxides, including nitrite. Although the interactions with trace nitrogen sources are limited, longer treatment times allow for gradual nitrite accumulation. Such extended plasma exposures will give more opportunities for any present nitrogen to react and form nitrites.

When comparing the nitrite concentrations observed in this study to values reported in previous studies (Table 2), it is evident that nitrite production in the submerged plasma set-up is significantly lower than in set-ups where plasma is generated above the liquid. The submerged configuration limits direct exposure of the plasma to atmospheric nitrogen, which is a crucial factor to initiate nitrite formation. The liquid environment may quench the reactive plasma species, thereby reducing their chemical reactivity by the time they reach the air above the liquid. Additionally, the argon gas used in this study (Alphagaz 1), is free from nitrogen impurities according to the manufacturer's specifications, further limiting the nitrogen available for nitrite production.

Chen *et al.* used a plasma jet submerged in liquid to treat deionized (DI) water with various gases, including industrial-grade He, argon, and He. These studies indicate that nitrite concentrations were low in a submerged set-up, aligning with the results of this study. However, their findings showed higher nitrite concentrations compared to our study, likely due to nitrogen impurities in the industrial-grade gases. Furthermore, the gap between the plasma nozzle and liquid surface also plays

a crucial role in nitrite formation, although this was not specified in their set-up [21] [22].

In summary, this study highlights significant impact of plasma configuration on nitrite production in plasma-treated liquids. The submerged Ar plasma jet set-up used here, characterized by its limited nitrogen source and reduced interaction with atmospheric nitrogen, produces notably lower nitrite concentrations compared to configurations where plasma is generated above the liquid surface. Although nitrite levels increase linearly with longer plasma exposure, overall production is constrained by the experimental conditions, with gas flow rate and applied voltage showing minimal influence.

E. pH

Besides the chemical composition, plasma treatment can also affect the physical characteristics of the liquid, such as pH.

To determine plasma treatment induced alterations in the acidity level of the plasma-treated PBS, pH measurements were conducted under varying voltage, gas flow rate, and exposure time. The findings, depicted in Figure 4 (g – i), show that the pH remains relatively stable (close to 7.7), across all plasma operational parameters. This stability in pH can be attributed to the buffering properties of PBS, which help maintain an osmolarity comparable to that of the human body [39]. This is an advantage of using PBS instead of non-buffered solutions, which are known to acidify significantly upon plasma treatment, due to the generation of nitrate and nitrite ions [113] [114]. Such acidic liquids have a negative impact on healthy cells and compromise the selectivity of PTLs against cancer cells. Some studies have reported PBS acidification post-treatment [6] [115], typically when the production of hydrogen ions (H^+) during plasma treatment surpasses the buffering capacity of the PBS. However, in this study, the pH remained stable across all plasma operational parameters, highlighting the effectiveness of the liquid-submerged plasma set-up in preserving the buffering capacity of PBS.

The results of other characteristics of plasma-treated PBS, including conductivity, temperature, and liquid volume loss post-treatment, are provided in the Supplementary material as a function of plasma operational parameters, along with the corresponding materials and methods.

F. Conductivity

The conductivity of plasma-treated PBS was also examined as a function of voltage, flow rate and exposure time, as presented in Figure 5. The initial conductivity of untreated PBS was 15.8 ± 0.19 mS/cm, and plasma treatment consistently increased this value with higher voltage, gas flow rate, and treatment time.

This increase in conductivity can be attributed to the dissolution of charged species and ionic compounds generated during plasma exposure, which is a well-documented phenomenon in PTLs [116]. Notably, long-lived ionic species, such as NO_2^- and NO_3^-, substantially contribute to this conductivity enhancement [117] [118] [119]. In this study, NO_2^- emerged as the predominant long-lived ionic species, and its accumulation is directly correlated with increasing conductivity in plasma-treated PBS. Nevertheless, as discussed in Section 3.5, NO_2^- concentrations remain relatively stable across different flow rates and voltages, with significant increases occurring only with prolonged exposure times. Additionally, the overall nitrite concentrations observed in this study were relatively low.

However, H_2O_2, albeit recognized as a weak electrolyte, can also influence electrical conductivity [120]. Wu *et al.* [118] observed that conductivity in H_2O_2-enhanced plasma-treated water increased with rising H_2O_2 concentrations. The high H_2O_2 concentrations generated in this study are likely to contribute to the observed conductivity increases, as a function of voltage and exposure time. Furthermore, while variations in gas flow rate do not markedly affect the generation of RONS, the observed conductivity changes under different flow rates can be attributed to evaporation effects. Evaporation reduces the water content, thereby increasing the concentration of soluble salts in the PBS, which, in turn, increases conductivity. This is supported by data indicating increased liquid loss under high flow rates, as shown in Supplementary Figure 3. Similar evaporation effects were also observed with increasing voltage and plasma exposure time. Overall, it is important to note that the measured conductivities remain within physiological ranges [121], highlighting the relevance of the plasma-treated solutions in this study within the context of plasma medicine.

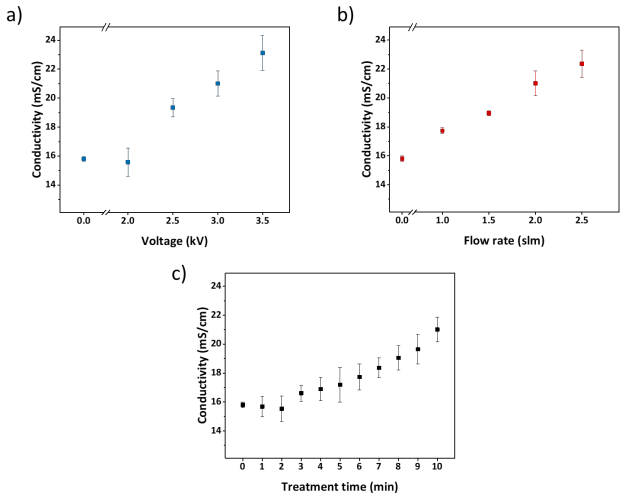

Figure 5: Conductivity of plasma-treated PBS for various (a) voltages, (b) flow rates, and (c) treatment times.

In summary, the observed increase in conductivity of plasma-treated PBS can be attributed to the dissolution of charged species and ionic compounds, particularly NO_2^- and H_2O_2, as well as the concentration effects of salts resulting from evaporation during plasma treatment. These factors collectively enhance the electrical properties of plasma-treated PBS.

G. PTL aging effect

The stability of the generated RONS species in PTLs is crucial, as delays between their generation and application

could compromise their anti-cancer efficacy. A reduction in the RONS concentrations during storage will negatively impact the therapeutic efficacy of the PTLs and should be therefore minimized. In this study, the stability of plasma-treated PBS using the following parameters was examined: voltage of 3.0 kV, flow rate of 2.0 slm, and a treatment time of 10 minutes. This specific parametric configuration was selected due to its optimal balance between high RONS concentration and acceptable liquid loss. It is well known that higher concentrations of reactive species accelerate the aging process of PTLs [31], rendering this specific configuration highly relevant for studying RONS stability. The plasma-treated PBS was stored at 3 different temperatures (4, 21 and 37°C) over a 21-day period, with stability assays conducted every 7 days. At each time point, H_2O_2 and nitrite concentrations in the liquid were determined.

Figure 6 (a) shows the evolution of the H_2O_2 concentration over time for the 3 storage temperatures. The results show that at 4°C and 21°C, the H_2O_2 concentration remained stable or even slightly increased after 2 and 3 weeks of storage. This unexpected increase was also observed by Zhao *et al.* who reported a significant 303% increase in H_2O_2 concentration after 48 hours of storage at 4°C [122]. However, the specific mechanisms leading to the increase of H_2O_2 in plasma-treated PBS in this study remain unknown.

In contrast, at 37°C, the H_2O_2 concentration tends to slightly decrease over time, diminishing by 2.8% after 3 weeks of storage. From a thermodynamic perspective, the stability of H_2O_2 is influenced by temperature, as its decomposition rate is highly temperature-dependent, with higher temperatures accelerating its breakdown [113]. Given that the pH of the plasma-treated PBS remains stable after plasma exposure due to the buffering effect of PBS, the observed decline in H_2O_2 concentration at 37°C is likely mainly deriven by thermal decomposition. The high stability of H_2O_2 in plasma-treated PBS is in excellent agreement with other studies on the storage of plasma-treated PBS [115] [123]. The consistent H_2O_2 levels in plasma-treated PBS stored at ≤ 21°C highlight its potential as a stable and reliable medium for cancer treatment. Conversely, this high stability has not been observed in other liquids such as DMEM, where a significant decrease in H_2O_2 concentration was noted after 26 hours of storage, evidencing the unique stability of plasma-treated PBS [123]. The degradation of H_2O_2 in liquids containing proteins, metallic compounds (e.g. ferrous ions), amino acids, and glucose further supports the distinct advantages of using PBS as a plasma-treated medium [123] [124].

Figure 6 (b) depicts the variation in nitrite concentration over storage time for the 3 different storage temperatures. Similar trends as for the H_2O_2 concentration can be found as a function of storage time and storage temperature: (1) at temperatures below 21°C, the nitrite concentration remains stable over time and (2) at a temperature of 37°C, the nitrite concentration only slightly decreases at longer storage periods. While nitrite is generally stable, it is still subject to temperature-dependent changes. Additionally, higher initial concentrations of reactive species can accelerate decomposition reactions, whereas lower concentrations result in more moderate reactions promoting the stability of active species [31]. These observations are consistent with a study by Kutasi *et al.*, who have reported stable nitrite concentrations in plasma-treated PBS stored at 4°C for up to 4 months [125].

Nitrite stability is known to decrease under acidic conditions [126]; however, the almost neutral pH in this study, along with low storage temperatures, supported the extended preservation of nitrite in plasma-treated PBS. The buffering effect of PBS reduces the probability of nitrites reacting with H_2O_2 to form peroxynitrous acid or decomposing into nitric oxide and nitrogen dioxide [126].

To conclude, the results of this study reveal excellent long-term stability of both H_2O_2 and nitrite in plasma-treated PBS when stored at low temperatures. This stability is important for maintaining the therapeutic efficacy of PTLs in cancer treatment, making plasma-treated PBS a practical and effective medium for these applications.

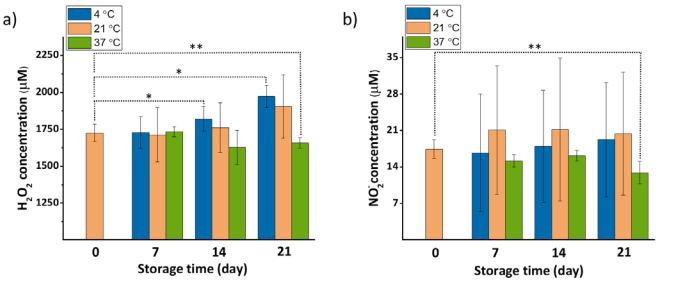

Figure 6. Evolution of (a) H_2O_2 concentration and (b) NO_2^- concentration of plasma-treated PBS (voltage: 3.0 kV, flow rate: 2.0 slm, treatment time: 10 min). Samples were stored at 4˚C, 21˚C, and 37˚C. A t-test was performed to check for statistical significance (*p ≤ 0.05, **p ≤ 0.01), determining differences in concentrations due to storage period and temperature variations.

H. Cell viability

Emerging literature has highlighted the therapeutic promise of PTLs in oncology, focusing on its selective cytotoxicity towards malignant cells [13] [32] [127]. In this section, the effects of 3-minute plasma-treated PBS (voltage: 3.0 kV, flow rate: 2.0 slm) on the proliferation and viability of OSCC versus non-malignant HaCaT cells were assessed. As control samples, different liquids were included: untreated PBS, PBS exposed to argon gas (without plasma), and PBS supplemented with exogenous H_2O_2, NO_2^-, and H_2O_2 + NO_2^- at concentrations matching those in plasma-treated PBS. The intermediate treatment duration of 3 minutes, that ensured significant RONS generation while minimizing liquid loss, was selected to reach an initial proof-of-concept of the potential efficacy of plasma-treated PBS. Upon successful completion of this initial study, future research will explore extended treatment durations to further assess its therapeutic potential.

As shown in Figure 7 (a), OSCC cells exhibited a marked reduction in proliferation post-incubation with plasma-treated PBS compared to the gas control and NO_2^--rich PBS, which became evident after 48 hours and further accentuated at 72

hours. In contrast, HaCaT cells maintained a stable proliferation across all experimental conditions, indicating selective cytotoxicity of plasma-treated PBS towards OSCC cells.

Parallel to these findings, Figure 7 (b) illustrates similar results in viability, with plasma-treated PBS causing a significant reduction in OSCC cell viability to 50% at 24 hours and approximately 18% at 72 hours. OSCC cells incubated with the gas control sample and the NO_2^--rich PBS exhibited no decline in viability, suggesting that H_2O_2 is the dominant species inducing cancer cell death while nitrite has minimal impact. Other studies have also reported that H_2O_2 is most likely the dominant RONS responsible for inducing cancer cell death when using PTLs [22] [32] [37]. Notably, OSCC cells exposed to H_2O_2-rich or H_2O_2 + NO_2^--rich PBS showed higher viability compared to plasma-treated PBS, emphasizing the superior efficacy of plasma-treated PBS in targeting cancer cells over merely adding exogenous chemicals. This indicates that additional RONS contribute synergistically to the cytotoxicity of plasma-treated PBS, reinforcing the significance of using PTLs over reconstituted controls. Moreover, Pavlik et al. [86] demonstrated that while both PTLs and chemically prepared solutions exhibit cytotoxic and genotoxic effects on K562 leukemia cells, their mechanisms of action differ. Specifically, PTLs induce apoptosis, whereas reconstituted controls primarily trigger necrosis, which is likely associated with increased inflammation and reduced therapeutic benefits. Further investigations into the death mechanisms induced by PTLs and reconstituted controls in OSCC cells will be conducted to elucidate their distinct biological effects. HaCaT cells exhibited no significant changes in viability across all treatments.

Plasma-treated PBS selectively inhibits OSCC cell proliferation and viability while sparing non-cancerous HaCaT cells. The exposure to plasma-treated PBS containing high levels of RONS, elevates the intracellular ROS in OSCC cells that already contain a higher ROS level compared to healthy cells. This elevated intracellular ROS level ultimately leads to DNA damage and cell death [128] [129]. Healthy cells, with lower baseline ROS levels and intact antioxidant systems [45], remain unaffected. This selective effect highlights the potential of plasma-treated PBS as a targeted cancer therapy. While promising, further studies are needed to confirm its anti-tumor efficacy. Specifically, it is essential to establish whether the treatment induces apoptosis whereby the necrotic damage and inflammation can be circumvented in oral cancer cells.

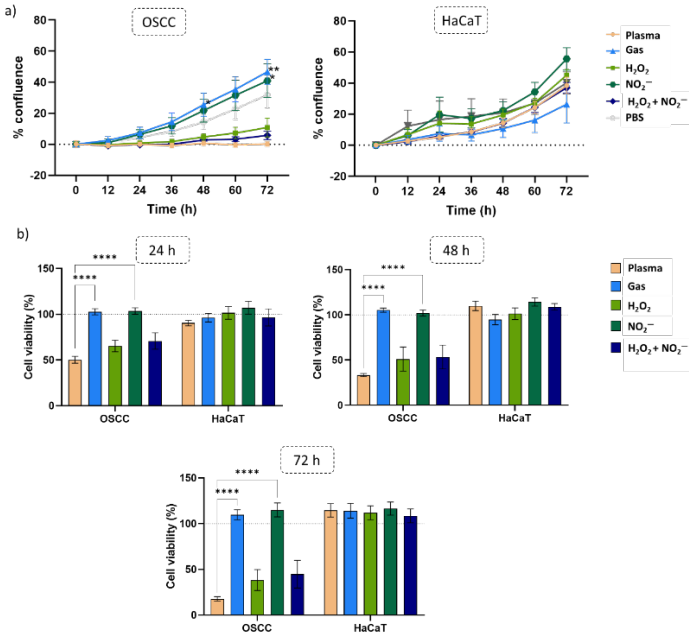

Figure 7. (a) Cell proliferation of cancer cells (OSCC) and healthy control cells (HaCaT) following exposure to plasma-treated PBS and corresponding controls over 72 h. (b) Cell viability after 24 h, 48 h and 72 h. N=3, with 3 technical replicates, *p ≤ 0.05, **p ≤ 0.01 ,**** p ≤ 0.0001.

IV. Conclusion

This study introduced a novel set-up using an argon plasma jet submerged in liquid to explore the physicochemical properties and anti-cancer efficacy of plasma-treated PBS. Key operational parameters, including voltage, gas flow rate, and treatment duration, were investigated for their impact on plasma properties and liquid characteristics. Results revealed that an increased voltage led to a higher discharge power due to intensified plasma generation and ionization levels. In contrast, changes in gas flow rate had a minimal impact on the discharge power. OES analysis identified critical radiative species in plasma such as excited Ar atoms, N_2, N_2^+, $^{\bullet}OH$ radicals, and atomic oxygen. Concerning the physiological properties of PBS, plasma exposure increased PBS temperature and liquid loss, with both the voltage and treatment duration significantly influencing these effects. The gas flow rate enhanced the liquid evaporation but had a lower impact on the PBS temperature. The pH of the plasma-treated PBS remained relatively consistent across all experimental conditions due to the PBS' buffering capacity thus preserving the liquid's physiological properties. In contrast, all operational parameters significantly impacted the conductivity of plasma-treated PBS due to the dissolution of charged species and increase in salt concentration as a result of evaporation. The H_2O_2 concentrations produced in this study were remarkably high, reaching up to 2000 µM depending on the operational parameters. Increased voltage raised plasma power and electron density, enhancing the electron impact dissociation of water into $^{\bullet}OH$ radicals, thus producing more H_2O_2. Extended treatment times further increased water molecule dissociation due to prolonged contact

with plasma species, resulting in higher H_2O_2 levels. Conversely, gas flow rate did not significantly impact H_2O_2 concentrations. In contrast, nitrite generation was relatively modest and not significantly affected by changes in voltage or gas flow rate. As plasma was submerged in the liquid, the liquid acted as a barrier, limiting reactive species from reaching its surface. However, nitrite concentration increased linearly with longer treatment times, as prolonged contact with plasma provided more opportunities for nitrogen to react and form nitrites. The stability of plasma-treated PBS was evaluated upon storage of PBS at 4°C, 21°C, and 37°C over 21 days. H_2O_2 and nitrite concentrations remained stable at lower temperatures, while higher temperatures accelerated their decomposition. Finally, plasma-treated PBS inhibited OSCC cell proliferation and viability without affecting healthy HaCaT cells. A comparison with PBS controls supplemented with exogenous H_2O_2, NO_2^-, and H_2O_2 + NO_2^- showed that H_2O_2 was the main cytotoxic and anti-proliferative agent in the plasma-treated PBS generated in this study, with NO_2^- having a minimal role.

In summary, PBS plasma-treated using a new liquid-submerged set-up shows potential as a selective and effective therapeutic strategy for targeting OSCC, offering a promising approach for cancer therapy.

ACKNOWLEDGMENT

PS and NDG acknowledge the support of the Special Research Fund of Ghent University in financing the interdisciplinary project 01IO2018. MN also acknowledges the support of the Special Research Fund of Ghent University in financing her postdoctoral position (01P06122). All authors declare that they have no known conflicts of interest in terms of competing financial interests or personal relationships that could have an influence or are relevant to the work reported in this paper.

REFERENCES

[1] K. Sklias, J. S. Sousa, and P. M. Girard, “Role of short- and long-lived reactive species on the selectivity and anti-cancer action of plasma treatment in vitro,” *Cancers (Basel).*, vol. 13, no. 4, pp. 1–31, 2021, doi: 10.3390/cancers13040615.

[2] H. Sung *et al.*, “Global Cancer Statistics 2020: GLOBOCAN Estimates of Incidence and Mortality Worldwide for 36 Cancers in 185 Countries,” *CA. Cancer J. Clin.*, vol. 71, no. 3, pp. 209–249, May 2021, doi: 10.3322/caac.21660.

[3] D. Yan, J. H. Sherman, and M. Keidar, “Cold atmospheric plasma, a novel promising anti-cancer treatment modality,” *Oncotarget*, vol. 8, no. 9, pp. 15977–15995, Feb. 2017, doi: 10.18632/oncotarget.13304.

[4] D. Yan, A. Horkowitz, Q. Wang, and M. Keidar, “On the selective killing of cold atmospheric plasma cancer treatment: Status and beyond,” *Plasma Process. Polym.*, vol. 18, no. 10, Oct. 2021, doi: 10.1002/ppap.202100020.

[5] F. Judée, C. Fongia, B. Ducommun, M. Yousfi, V. Lobjois, and N. Merbahi, “Short and long time effects of low temperature Plasma Activated Media on 3D multicellular tumor spheroids,” *Sci. Rep.*, vol. 6, no. 1, p. 21421, Feb. 2016, doi: 10.1038/srep21421.

[6] P.-M. Girard *et al.*, “Synergistic Effect of H2O2 and NO2 in Cell Death Induced by Cold Atmospheric He Plasma,” *Sci. Rep.*, vol. 6, no. 1, p. 29098, Jul. 2016, doi: 10.1038/srep29098.

[7] C. Labay *et al.*, “Enhanced Generation of Reactive Species by Cold Plasma in Gelatin Solutions for Selective Cancer Cell Death,” *ACS Appl. Mater. Interfaces*, vol. 12, no. 42, pp. 47256–47269, Oct. 2020, doi: 10.1021/acsami.0c12930.

[8] A. Lin, E. Biscop, Y. Gorbanev, E. Smits, and A. Bogaerts, “Toward defining plasma treatment dose: The role of plasma treatment energy of pulsed-dielectric barrier discharge in dictating in vitro biological responses,” *Plasma Process. Polym.*, vol. 19, no. 3, Mar. 2022, doi: 10.1002/ppap.202100151.

[9] N. Kaushik *et al.*, “Plasma and Nanomaterials: Fabrication and Biomedical Applications,” *Nanomaterials*, vol. 9, no. 1, p. 98, Jan. 2019, doi: 10.3390/nano9010098.

[10] H. Tanaka *et al.*, “Non-thermal atmospheric pressure plasma activates lactate in Ringer’s solution for anti-tumor effects,” *Sci. Rep.*, vol. 6, no. 1, p. 36282, Nov. 2016, doi: 10.1038/srep36282.

[11] J. Tornin, M. Mateu-Sanz, A. Rodríguez, C. Labay, R. Rodríguez, and C. Canal, “Pyruvate Plays a Main Role in the Antitumoral Selectivity of Cold Atmospheric Plasma in Osteosarcoma,” *Sci. Rep.*, vol. 9, no. 1, p. 10681, Jul. 2019, doi: 10.1038/s41598-019-47128-1.

[12] A. Privat-Maldonado, Y. Gorbanev, S. Dewilde, E. Smits, and A. Bogaerts, “Reduction of Human Glioblastoma Spheroids Using Cold Atmospheric Plasma: The Combined Effect of Short- and Long-Lived Reactive Species,” *Cancers (Basel).*, vol. 10, no. 11, p. 394, Oct. 2018, doi: 10.3390/cancers10110394.

[13] C. Canal, R. Fontelo, I. Hamouda, J. Guillem-Marti, U. Cvelbar, and M.-P. Ginebra, “Plasma-induced selectivity in bone cancer cells death,” *Free Radic. Biol. Med.*, vol. 110, no. May, pp. 72–80, Sep. 2017, doi: 10.1016/j.freeradbiomed.2017.05.023.

[14] H. Zhang *et al.*, “Antitumor effects of hyperthermia with plasma-treated solutions on 3D bladder tumor spheroids,” *Plasma Process. Polym.*, vol. 18, no. 10, pp. 1–8, Oct. 2021, doi: 10.1002/ppap.202100070.

[15] K. D. Weltmann, E. Kinde, T. Von Woedtke, M. Hähnel, M. Stieber, and R. Brandenburg, “Atmospheric-pressure plasma sources: Prospective tools for plasma medicine,” *Pure Appl. Chem.*, vol. 82, no. 6, pp. 1223–1237, 2010, doi: 10.1351/PAC-CON-09-10-35.

[16] H. Zhang *et al.*, “Plasma-activated thermosensitive biogel as an exogenous ROS carrier for post-surgical treatment of cancer,” *Biomaterials*, vol. 276, no. July, p. 121057, Sep. 2021, doi: 10.1016/j.biomaterials.2021.121057.

[17] H. Tanaka, S. Bekeschus, D. Yan, M. Hori, M. Keidar, and M. Laroussi, “Plasma-Treated Solutions (PTS) in Cancer Therapy,” *Cancers (Basel).*, vol. 13, no. 7, p. 1737, Apr. 2021, doi: 10.3390/cancers13071737.

[18] M. O. Oztan, U. K. Ercan, A. Aksoy Gokmen, F. Simsek, G. D. Ozdemir, and G. Koyluoglu, “Irrigation of peritoneal cavity with cold atmospheric plasma treated solution effectively reduces microbial load in rat acute peritonitis model,” *Sci. Rep.*, vol. 12, no. 1, p. 3646, Mar. 2022, doi: 10.1038/s41598-022-07598-2.

[19] X. Solé-Martí, A. Espona-Noguera, M.-P. Ginebra, and C. Canal, “Plasma-Conditioned Liquids as Anticancer Therapies In Vivo: Current State and Future Directions,” *Cancers (Basel).*, vol. 13, no. 3, p. 452, Jan. 2021, doi: 10.3390/cancers13030452.

[20] L. Miebach, E. Freund, R. Clemen, S. Kersting, L.-I. Partecke, and S. Bekeschus, “Gas plasma–oxidized sodium chloride acts via hydrogen peroxide in a model of peritoneal carcinomatosis,” *Proc. Natl. Acad. Sci.*, vol. 119, no. 31, Aug. 2022, doi: 10.1073/pnas.2200708119.

[21] Z. Chen, L. Lin, X. Cheng, E. Gjika, and M. Keidar, “Effects of cold atmospheric plasma generated in deionized water in cell cancer therapy,” *Plasma Process. Polym.*, vol. 13, no. 12, pp. 1151–1156, Dec. 2016, doi: 10.1002/ppap.201600086.

[22] Z. Chen, X. Cheng, L. Lin, and M. Keidar, “Cold atmospheric plasma discharged in water and its potential use in cancer therapy,” *J. Phys. D. Appl. Phys.*, vol. 50, no. 1, p. 015208, Jan. 2017, doi: 10.1088/1361-6463/50/1/015208.

[23] T. R. Brubaker *et al.*, “Dynamic analysis of reactive oxygen nitrogen species in plasma-activated culture medium by UV absorption spectroscopy,” *J. Appl. Phys.*, vol. 122, no. 21, Dec. 2017, doi: 10.1063/1.4999256.

[24] M. Meyer, G. Nayak, P. J. Bruggeman, and M. J. Kushner, “Sheath formation around a dielectric droplet in a He atmospheric pressure plasma,” *J. Appl. Phys.*, vol. 132, no. 8, Aug. 2022, doi: 10.1063/5.0103446.

[25] A. Mai-Prochnow *et al.*, “Interactions of plasma-activated water with biofilms: inactivation, dispersal effects and mechanisms of action,” *npj Biofilms Microbiomes*, vol. 7, no. 1, p. 11, Jan. 2021,

doi: 10.1038/s41522-020-00180-6.

[26] C. A. J. van Gils, S. Hofmann, B. K. H. L. Boekema, R. Brandenburg, and P. J. Bruggeman, "Mechanisms of bacterial inactivation in the liquid phase induced by a remote RF cold atmospheric pressure plasma jet," *J. Phys. D. Appl. Phys.*, vol. 46, no. 17, p. 175203, May 2013, doi: 10.1088/0022-3727/46/17/175203.

[27] J. Chauvin, F. Judée, M. Yousfi, P. Vicendo, and N. Merbahi, "Analysis of reactive oxygen and nitrogen species generated in three liquid media by low temperature helium plasma jet," *Sci. Rep.*, vol. 7, no. 1, p. 4562, Jul. 2017, doi: 10.1038/s41598-017-04650-4.

[28] I.-E. Vlad and S. D. Anghel, "Time stability of water activated by different on-liquid atmospheric pressure plasmas," *J. Electrostat.*, vol. 87, pp. 284–292, Jun. 2017, doi: 10.1016/j.elstat.2017.06.002.

[29] J.-S. Oh *et al.*, "UV–vis spectroscopy study of plasma-activated water: Dependence of the chemical composition on plasma exposure time and treatment distance," *Jpn. J. Appl. Phys.*, vol. 57, no. 1, p. 0102B9, Jan. 2018, doi: 10.7567/JJAP.57.0102B9.

[30] Z. Chen *et al.*, "Analysis of the production mechanism of H 2 O 2 in water treated by helium DC plasma jets," *J. Phys. D. Appl. Phys.*, vol. 51, no. 32, p. 325201, Aug. 2018, doi: 10.1088/1361-6463/aad0eb.

[31] K. Kutasi, D. Popović, N. Krstulović, and S. Milošević, "Tuning the composition of plasma-activated water by a surface-wave microwave discharge and a kHz plasma jet," *Plasma Sources Sci. Technol.*, vol. 28, no. 9, p. 095010, Sep. 2019, doi: 10.1088/1361-6595/ab3c2f.

[32] D. Sersenová, Z. Machala, V. Repiská, and H. Gbelcová, "Selective Apoptotic Effect of Plasma Activated Liquids on Human Cancer Cell Lines," *Molecules*, vol. 26, no. 14, p. 4254, Jul. 2021, doi: 10.3390/molecules26144254.

[33] L. Miebach, E. Freund, R. Clemen, S. Kersting, L.-I. Partecke, and S. Bekeschus, "Gas plasma–oxidized sodium chloride acts via hydrogen peroxide in a model of peritoneal carcinomatosis," *Proc. Natl. Acad. Sci.*, vol. 119, no. 31, pp. 1–10, Aug. 2022, doi: 10.1073/pnas.2200708119.

[34] Z. Liu *et al.*, "The impact of surface-to-volume ratio on the plasma activated water characteristics and its anticancer effect," *J. Phys. D. Appl. Phys.*, vol. 54, no. 21, p. 215203, May 2021, doi: 10.1088/1361-6463/abe78f.

[35] M. Janda, A. Stancampiano, F. di Natale, and Z. Machala, "Short Review on Plasma–Aerosol Interactions," *Plasma Process. Polym.*, vol. 22, no. 1, Jan. 2025, doi: 10.1002/ppap.202400275.

[36] M. J. Traylor *et al.*, "Long-term antibacterial efficacy of air plasma-activated water," *J. Phys. D. Appl. Phys.*, vol. 44, no. 47, p. 472001, Nov. 2011, doi: 10.1088/0022-3727/44/47/472001.

[37] W. Van Boxem *et al.*, "Anti-cancer capacity of plasma-treated PBS: effect of chemical composition on cancer cell cytotoxicity," *Sci. Rep.*, vol. 7, no. 1, p. 16478, Nov. 2017, doi: 10.1038/s41598-017-16758-8.

[38] E. Griseti, N. Merbahi, and M. Golzio, "Anti-Cancer Potential of Two Plasma-Activated Liquids: Implication of Long-Lived Reactive Oxygen and Nitrogen Species," *Cancers (Basel).*, vol. 12, no. 3, p. 721, Mar. 2020, doi: 10.3390/cancers12030721.

[39] E. Griseti, N. Merbahi, and M. Golzio, "Anti-cancer potential of two plasma-activated liquids: Implication of long-lived reactive oxygen and nitrogen species," *Cancers (Basel).*, vol. 12, no. 3, 2020, doi: 10.3390/cancers12030721.

[40] J. Tornín *et al.*, "Cold plasma and inhibition of STAT3 selectively target tumorigenicity in osteosarcoma," *Redox Biol.*, vol. 62, p. 102685, Jun. 2023, doi: 10.1016/j.redox.2023.102685.

[41] A. S. Gubarev *et al.*, "Conformational Parameters and Hydrodynamic Behavior of Poly(2-Methyl-2-Oxazoline) in a Broad Molar Mass Range," *Polymers (Basel).*, vol. 15, no. 3, p. 623, Jan. 2023, doi: 10.3390/polym15030623.

[42] American Cancer Society, "Survival Rates for Oral Cavity and Oropharyngeal Cancer." [Online]. Available: https://www.cancer.org/cancer/types/oral-cavity-and-oropharyngeal-cancer/detection-diagnosis-staging/survival-rates.html

[43] S. C. H. Cheng, V. W. C. Wu, D. L. W. Kwong, and M. T. C. Ying, "Assessment of post-radiotherapy salivary glands," *Br. J. Radiol.*, vol. 84, no. 1001, pp. 393–402, May 2011, doi: 10.1259/bjr/66754762.

[44] A. K. Markopoulos, "Current Aspects on Oral Squamous Cell Carcinoma," *Open Dent. J.*, vol. 6, no. 1, pp. 126–130, Aug. 2012, doi: 10.2174/1874210601206010126.

[45] A. Kesarwala, M. Krishna, and J. Mitchell, "Oxidative stress in oral diseases," *Oral Dis.*, vol. 22, no. 1, pp. 9–18, Jan. 2016, doi: 10.1111/odi.12300.

[46] J. B. Fox, "Kinetics and mechanisms of the Griess reaction," *Anal. Chem.*, vol. 51, no. 9, pp. 1493–1502, Aug. 1979, doi: 10.1021/ac50045a032.

[47] W. P. Robarge, A. Edwards, and B. Johnson, "Water and waste water analysis for nitrate via nitration of salicylic acid," *Commun. Soil Sci. Plant Anal.*, vol. 14, no. 12, pp. 1207–1215, Dec. 1983, doi: 10.1080/00103628309367444.

[48] X. Lu, G. V. Naidis, M. Laroussi, S. Reuter, D. B. Graves, and K. Ostrikov, "Reactive species in non-equilibrium atmospheric-pressure plasmas: Generation, transport, and biological effects," *Phys. Rep.*, vol. 630, pp. 1–84, May 2016, doi: 10.1016/j.physrep.2016.03.003.

[49] Y. R. Zhang, K. Van Laer, E. C. Neyts, and A. Bogaerts, "Can plasma be formed in catalyst pores? A modeling investigation," *Appl. Catal. B Environ.*, vol. 185, pp. 56–67, 2016, doi: 10.1016/j.apcatb.2015.12.009.

[50] A. Van Deynse, P. Cools, C. Leys, N. De Geyter, and R. Morent, "Surface activation of polyethylene with an argon atmospheric pressure plasma jet: Influence of applied power and flow rate," *Appl. Surf. Sci.*, vol. 328, pp. 269–278, 2015, doi: 10.1016/j.apsusc.2014.12.075.

[51] I. Sremački *et al.*, "On diagnostics of annular-shape radio-frequency plasma jet operating in argon in atmospheric conditions," *Plasma Sources Sci. Technol.*, vol. 29, no. 3, p. 035027, Mar. 2020, doi: 10.1088/1361-6595/ab71f7.

[52] L. Taghizadeh, G. Brackman, A. Nikiforov, J. van der Mullen, C. Leys, and T. Coenye, "Inactivation of Biofilms Using a Low Power Atmospheric Pressure Argon Plasma Jet; the Role of Entrained Nitrogen," *Plasma Process. Polym.*, vol. 12, no. 1, pp. 75–81, Jan. 2015, doi: 10.1002/ppap.201400074.

[53] D. L. Crintea, U. Czarnetzki, S. Iordanova, I. Koleva, and D. Luggenhölscher, "Plasma diagnostics by optical emission spectroscopy on argon and comparison with Thomson scattering," *J. Phys. D. Appl. Phys.*, vol. 42, no. 4, p. 045208, Feb. 2009, doi: 10.1088/0022-3727/42/4/045208.

[54] A. Sarani, A. Y. Nikiforov, and C. Leys, "Atmospheric pressure plasma jet in Ar and Ar/H2O mixtures: Optical emission spectroscopy and temperature measurements," *Phys. Plasmas*, vol. 17, no. 6, pp. 0–8, Jun. 2010, doi: 10.1063/1.3439685.

[55] N. Bolouki, W.-H. Kuan, Y.-Y. Huang, and J.-H. Hsieh, "Characterizations of a Plasma-Water System Generated by Repetitive Microsecond Pulsed Discharge with Air, Nitrogen, Oxygen, and Argon Gases Species," *Appl. Sci.*, vol. 11, no. 13, p. 6158, Jul. 2021, doi: 10.3390/app11136158.

[56] K. Gazeli, P. Svarnas, B. Held, L. Marlin, and F. Clément, "Possibility of controlling the chemical pattern of He and Ar 'guided streamers' by means of N2 or O2 additives," *J. Appl. Phys.*, vol. 117, no. 9, 2015, doi: 10.1063/1.4914035.

[57] V. V. Kovačević, B. P. Dojčinović, M. Jović, G. M. Roglić, B. M. Obradović, and M. M. Kuraica, "Measurement of reactive species generated by dielectric barrier discharge in direct contact with water in different atmospheres," *J. Phys. D. Appl. Phys.*, vol. 50, no. 15, 2017, doi: 10.1088/1361-6463/aa5fde.

[58] Q. Xiong, A. Y. Nikiforov, X. P. Lu, and C. Leys, "High-speed dispersed photographing of an open-air argon plasma plume by a grating–ICCD camera system," *J. Phys. D. Appl. Phys.*, vol. 43, no. 41, p. 415201, Oct. 2010, doi: 10.1088/0022-3727/43/41/415201.

[59] R. S. Mangina, J. M. Ajello, R. A. West, and D. Dziczek, "HIGH-RESOLUTION ELECTRON-IMPACT EMISSION SPECTRA AND VIBRATIONAL EMISSION CROSS SECTIONS FROM 330–1100 nm FOR N 2," *Astrophys. J. Suppl. Ser.*, vol. 196, no. 1, p. 13, Sep. 2011, doi: 10.1088/0067-0049/196/1/13.

[60] P. Lamichhane, B. Ghimire, S. Mumtaz, R. Paneru, S. H. Ki, and E. H. Choi, "Control of hydrogen peroxide production in plasma activated water by utilizing nitrification," *J. Phys. D. Appl. Phys.*, vol. 52, no. 26, 2019, doi: 10.1088/1361-6463/ab16a9.

[61] B. Ghimire *et al.*, "Enhancement of hydrogen peroxide production from an atmospheric pressure argon plasma jet and implications to the antibacterial activity of plasma activated water," *Plasma Sources Sci. Technol.*, vol. 30, no. 3, 2021, doi: 10.1088/1361-6595/abe0c9.

[62] R. Ghobeira, P. S. Esbah Tabaei, A. Nikiforov, R. Morent, and N. De Geyter, “Unraveling Exclusive In-Plasma Initiated Oxidation Processes Occurring at Polymeric Surfaces upon O2 Admixtures to Medium Pressure Ar and N2 DBD Treatments,” *Polymers (Basel).*, vol. 15, no. 14, p. 2978, Jul. 2023, doi: 10.3390/polym15142978.

[63] D. Xiao *et al.*, “Characteristics of atmospheric-pressure non-thermal N 2 and N 2 /O 2 gas mixture plasma jet,” *J. Appl. Phys.*, vol. 115, no. 3, p. 033303, Jan. 2014, doi: 10.1063/1.4862304.

[64] N. K. Kaushik *et al.*, “Biological and medical applications of plasmaactivated,” *Biol. Chem.*, vol. 400, no. 1, pp. 39–62, 2018, doi: 10.1515/hsz-2018-0226.

[65] M. Mateu-Sanz *et al.*, “Cold Plasma-Treated Ringer’s Saline: A Weapon to Target Osteosarcoma,” *Cancers (Basel).*, vol. 12, no. 1, p. 227, Jan. 2020, doi: 10.3390/cancers12010227.

[66] A. Jo, H. M. Joh, T. H. Chung, and J. W. Chung, “Anticancer Effects of Plasma-Activated Medium Produced by a Microwave-Excited Atmospheric Pressure Argon Plasma Jet,” *Oxid. Med. Cell. Longev.*, vol. 2020, pp. 1–17, Jul. 2020, doi: 10.1155/2020/4205640.

[67] F. Virard, S. Cousty, J.-P. Cambus, A. Valentin, P. Kémoun, and F. Clément, “Cold Atmospheric Plasma Induces a Predominantly Necrotic Cell Death via the Microenvironment,” *PLoS One*, vol. 10, no. 8, p. e0133120, Aug. 2015, doi: 10.1371/journal.pone.0133120.

[68] C. Bradu, K. Kutasi, M. Magureanu, N. Puač, and S. Živković, “Reactive nitrogen species in plasma-activated water: generation, chemistry and application in agriculture,” *J. Phys. D. Appl. Phys.*, vol. 53, no. 22, p. 223001, May 2020, doi: 10.1088/1361-6463/ab795a.

[69] V. N. Ochkin, *Spectroscopy of Low Temperature Plasma*. Wiley, 2009. doi: 10.1002/9783527627509.

[70] Y. F. Yue, S. Mohades, M. Laroussi, and X. Lu, “Measurements of Plasma-Generated Hydroxyl and Hydrogen Peroxide Concentrations for Plasma Medicine Applications,” *IEEE Trans. Plasma Sci.*, vol. 44, no. 11, pp. 2754–2758, Nov. 2016, doi: 10.1109/TPS.2016.2550805.

[71] S. Schüttler, A. L. Schöne, E. Jeß, A. R. Gibson, and J. Golda, “Production and transport of plasma-generated hydrogen peroxide from gas to liquid,” *Phys. Chem. Chem. Phys.*, vol. 26, no. 10, pp. 8255–8272, 2024, doi: 10.1039/D3CP04290A.

[72] J. Patel and M. J. Keshvani, “Study of Plasma–Water Interactions: Effect of Plasma Electrons and Production of Hydrogen Peroxide,” *Russ. J. Phys. Chem. A*, vol. 95, no. 13, pp. 2691–2698, Dec. 2021, doi: 10.1134/S0036024421130161.

[73] W. Wang *et al.*, “Nitrox surface discharge used for water activation: The reactive species and their correlation to the bactericidal effect,” *J. Phys. D. Appl. Phys.*, vol. 55, no. 26, 2022, doi: 10.1088/1361-6463/ac61b1.

[74] B. R. Locke and K.-Y. Shih, “Review of the methods to form hydrogen peroxide in electrical discharge plasma with liquid water,” *Plasma Sources Sci. Technol.*, vol. 20, no. 3, p. 034006, Jun. 2011, doi: 10.1088/0963-0252/20/3/034006.

[75] S. Mohades, A. M. Lietz, J. Kruszelnicki, and M. J. Kushner, “Helium plasma jet interactions with water in well plates,” *Plasma Process. Polym.*, vol. 17, no. 3, pp. 1–17, Mar. 2020, doi: 10.1002/ppap.201900179.

[76] J. Winter *et al.*, “Tracking plasma generated H 2 O 2 from gas into liquid phase and revealing its dominant impact on human skin cells,” *J. Phys. D. Appl. Phys.*, vol. 47, no. 28, p. 285401, Jul. 2014, doi: 10.1088/0022-3727/47/28/285401.

[77] P. Attri and A. Bogaerts, “Perspectives of Plasma-treated Solutions as Anticancer Drugs,” *Anticancer. Agents Med. Chem.*, vol. 19, no. 4, pp. 436–438, Jun. 2019, doi: 10.2174/1871520619041905211023 45.

[78] E. Sardella *et al.*, “Plasma Treated Water Solutions in Cancer Treatments: The Contrasting Role of RNS,” *Antioxidants*, vol. 10, no. 4, p. 605, Apr. 2021, doi: 10.3390/antiox10040605.

[79] Y. Hu, S. Peng, W. Xi, Y. Lan, W. Han, and C. Cheng, “Study on the anticancer effect and mechanism of action of reactive species in plasma-activated solution against colorectal cancer cells,” *Plasma Process. Polym.*, vol. 21, no. 4, pp. 1–17, Apr. 2024, doi: 10.1002/ppap.202300175.

[80] J. M. Joslin, J. R. McCall, J. P. Bzdek, D. C. Johnson, and B. M. Hybertson, “Aqueous Plasma Pharmacy: Preparation Methods, Chemistry, and Therapeutic Applications,” *Plasma Med.*, vol. 6, no. 2, pp. 135–177, 2016, doi: 10.1615/PlasmaMed.2016018618.

[81] E. Tsoukou, P. Bourke, and D. Boehm, “Understanding the Differences Between Antimicrobial and Cytotoxic Properties of Plasma Activated Liquids,” *Plasma Med.*, vol. 8, no. 3, pp. 299–320, 2018, doi: 10.1615/PlasmaMed.2018028261.

[82] C. Lazzaroni, P. Chabert, M. A. Lieberman, A. J. Lichtenberg, and A. Leblanc, “Analytical–numerical global model of atmospheric-pressure radio-frequency capacitive discharges,” *Plasma Sources Sci. Technol.*, vol. 21, no. 3, p. 035013, Jun. 2012, doi: 10.1088/0963-0252/21/3/035013.

[83] P. Dimitrakellis, M. Giannoglou, Z. M. Xanthou, E. Gogolides, P. Taoukis, and G. Katsaros, “Application of plasma-activated water as an antimicrobial washing agent of fresh leafy produce,” *Plasma Process. Polym.*, vol. 18, no. 12, pp. 1–13, Dec. 2021, doi: 10.1002/ppap.202100030.

[84] N. Kurake *et al.*, “Cell survival of glioblastoma grown in medium containing hydrogen peroxide and/or nitrite, or in plasma-activated medium,” *Arch. Biochem. Biophys.*, vol. 605, pp. 102–108, Sep. 2016, doi: 10.1016/j.abb.2016.01.011.

[85] T. Adachi, H. Tanaka, S. Nonomura, H. Hara, S. Kondo, and M. Hori, “Plasma-activated medium induces A549 cell injury via a spiral apoptotic cascade involving the mitochondrial–nuclear network,” *Free Radic. Biol. Med.*, vol. 79, pp. 28–44, Feb. 2015, doi: 10.1016/j.freeradbiomed.2014.11.014.

[86] T. I. Pavlik, N. G. Gusein-zade, L. V. Kolik, and N. L. Shimanovskii, “Comparison of the Biological Properties of Plasma-Treated Solution and Solution of Chemical Reagents,” *Appl. Sci.*, vol. 12, no. 8, p. 3704, Apr. 2022, doi: 10.3390/app12083704.

[87] Z. Chen, L. Lin, E. Gjika, X. Cheng, J. Canady, and M. Keidar, “Selective Treatment of Pancreatic Cancer Cells by Plasma-Activated Saline Solutions,” *IEEE Trans. Radiat. Plasma Med. Sci.*, vol. 2, no. 2, pp. 116–120, Mar. 2018, doi: 10.1109/TRPMS.2017.2761192.

[88] Z. Chen *et al.*, “A Novel Micro Cold Atmospheric Plasma Device for Glioblastoma Both In Vitro and In Vivo,” *Cancers (Basel).*, vol. 9, no. 12, p. 61, May 2017, doi: 10.3390/cancers9060061.

[89] B. Ghimire, J. Sornsakdanuphap, Y. J. Hong, H. S. Uhm, K.-D. Weltmann, and E. H. Choi, “The effect of the gap distance between an atmospheric-pressure plasma jet nozzle and liquid surface on OH and N2 species concentrations,” *Phys. Plasmas*, vol. 24, no. 7, Jul. 2017, doi: 10.1063/1.4989735.

[90] J. Lim, E. J. Hong, S. B. Kim, and S. Ryu, “The Effect of Gap Distance between a Pin and Water Surface on the Inactivation of Escherichia coli Using a Pin-to-Water Plasma,” *Int. J. Mol. Sci.*, vol. 23, no. 10, p. 5423, May 2022, doi: 10.3390/ijms23105423.

[91] J. Anuntagool, N. Srangsomjit, P. Thaweewong, and G. Alvarez, “A review on dielectric barrier discharge nonthermal plasma generation, factors affecting reactive species, and microbial inactivation,” *Food Control*, vol. 153, no. December 2022, p. 109913, Nov. 2023, doi: 10.1016/j.foodcont.2023.109913.

[92] B. ZHANG, Y. ZHU, F. LIU, and Z. FANG, “The influence of grounded electrode positions on the evolution and characteristics of an atmospheric pressure argon plasma jet,” *Plasma Sci. Technol.*, vol. 19, no. 6, p. 064001, Jun. 2017, doi: 10.1088/2058-6272/aa629f.

[93] H. Tresp, M. U. Hammer, K.-D. Weltmann, and S. Reuter, “Effects of Atmosphere Composition and Liquid Type on Plasma-Generated Reactive Species in Biologically Relevant Solutions,” *Plasma Med.*, vol. 3, no. 1–2, pp. 45–55, 2013, doi: 10.1615/PlasmaMed.2014009711.

[94] M. Horiba, T. Kamiya, H. Hara, and T. Adachi, “Cytoprotective effects of mild plasma-activated medium against oxidative stress in human skin fibroblasts,” *Sci. Rep.*, vol. 7, no. 1, p. 42208, Feb. 2017, doi: 10.1038/srep42208.

[95] D. Boehm, J. Curtin, P. J. Cullen, and P. Bourke, “Hydrogen Peroxide and Beyond-the Potential of High-voltage Plasma-activated Liquids Against Cancerous Cells,” *Anticancer. Agents Med. Chem.*, vol. 18, no. 6, pp. 815–823, 2017, doi: 10.2174/1871520617666170801110517.

[96] G. Bauer, “Intercellular singlet oxygen-mediated bystander signaling triggered by long-lived species of cold atmospheric plasma and plasma-activated medium,” *Redox Biol.*, vol. 26, p. 101301, Sep. 2019, doi: 10.1016/j.redox.2019.101301.

[97] D. Sersenová, Z. Machala, V. Repiská, and H. Gbelcová, “The effect of plasma activated medium and PBS on human melanoma cells compared with other cancer and normal cells,” no. January, 2021, doi: 10.20944/preprints202101.0068.v1.

[98] M. J. Pavlovich, H.-W. Chang, Y. Sakiyama, D. S. Clark, and D. B. Graves, "Ozone correlates with antibacterial effects from indirect air dielectric barrier discharge treatment of water," *J. Phys. D. Appl. Phys.*, vol. 46, no. 14, p. 145202, Apr. 2013, doi: 10.1088/0022-3727/46/14/145202.

[99] M. Živanić *et al.*, "Injectable Plasma-Treated Alginate Hydrogel for Oxidative Stress Delivery to Induce Immunogenic Cell Death in Osteosarcoma," *Adv. Funct. Mater.*, vol. 34, no. 14, Apr. 2024, doi: 10.1002/adfm.202312005.

[100] G. Bauer, "The synergistic effect between hydrogen peroxide and nitrite, two long-lived molecular species from cold atmospheric plasma, triggers tumor cells to induce their own cell death," *Redox Biol.*, vol. 26, no. July, p. 101291, Sep. 2019, doi: 10.1016/j.redox.2019.101291.

[101] T. Zimmermann *et al.*, "Acidified Nitrite Contributes to the Antitumor Effect of Cold Atmospheric Plasma on Melanoma Cells," *Int. J. Mol. Sci.*, vol. 22, no. 7, p. 3757, Apr. 2021, doi: 10.3390/ijms22073757.

[102] P. Lukes, B. R. Locke, and J. Brisset, "Aqueous-Phase Chemistry of Electrical Discharge Plasma in Water and in Gas–Liquid Environments," in *Plasma Chemistry and Catalysis in Gases and Liquids*, no. Chapter 6, Wiley, 2012, pp. 243–308. doi: 10.1002/9783527649525.ch7.

[103] R. Zhou *et al.*, "Plasma-activated water: generation, origin of reactive species and biological applications," *J. Phys. D. Appl. Phys.*, vol. 53, no. 30, p. 303001, Jul. 2020, doi: 10.1088/1361-6463/ab81cf.

[104] W. Van Gaens and A. Bogaerts, "Reaction pathways of biomedically active species in an Ar plasma jet," *Plasma Sources Sci. Technol.*, vol. 23, no. 3, p. 035015, May 2014, doi: 10.1088/0963-0252/23/3/035015.

[105] R. J. Wandell, H. Wang, R. K. M. Bulusu, R. O. Gallan, and B. R. Locke, "Formation of Nitrogen Oxides by Nanosecond Pulsed Plasma Discharges in Gas–Liquid Reactors," *Plasma Chem. Plasma Process.*, vol. 39, no. 3, pp. 643–666, May 2019, doi: 10.1007/s11090-019-09981-w.

[106] A. J. Wagner, D. H. Fairbrother, and F. Reniers, "A Comparison of PE Surfaces Modified by Plasma Generated Neutral Nitrogen Species and Nitrogen Ions," *Plasmas Polym.*, vol. 8, no. 2, pp. 119–134, 2003, doi: 10.1023/A:1023942211714.

[107] A. Fierro, G. Laity, and A. Neuber, "Optical emission spectroscopy study in the VUV–VIS regimes of a developing low-temperature plasma in nitrogen gas," *J. Phys. D. Appl. Phys.*, vol. 45, no. 49, p. 495202, Dec. 2012, doi: 10.1088/0022-3727/45/49/495202.

[108] A. Kuklya, C. Engelhard, K. Kerpen, and U. Telgheder, "Spectroscopic characterization of a low-temperature plasma ambient ionization probe operated with helium/nitrogen plasma gas mixtures," *J. Anal. At. Spectrom.*, vol. 31, no. 8, pp. 1574–1581, 2016, doi: 10.1039/C6JA00148C.

[109] K. Hadinoto, B. A. Niemira, and F. J. Trujillo, "A review on plasma-activated water and its application in the meat industry," *Compr. Rev. Food Sci. Food Saf.*, vol. 22, no. 6, pp. 4993–5019, Nov. 2023, doi: 10.1111/1541-4337.13250.

[110] Z. Chen, L. Lin, X. Cheng, E. Gjika, and M. Keidar, "Treatment of gastric cancer cells with nonthermal atmospheric plasma generated in water," *Biointerphases*, vol. 11, no. 3, Sep. 2016, doi: 10.1116/1.4962130.

[111] H. S. Uhm, "Generation of various radicals in nitrogen plasma and their behavior in media," *Phys. Plasmas*, vol. 22, no. 12, Dec. 2015, doi: 10.1063/1.4936796.

[112] M. Gromov *et al.*, "Plasma-assisted nitrogen fixation: the effect of water presence," *Green Chem.*, vol. 24, no. 24, pp. 9677–9689, 2022, doi: 10.1039/D2GC03063B.

[113] B. Pang *et al.*, "Investigation of the chemical characteristics and anticancer effect of plasma-activated water: The effect of liquid temperature," *Plasma Process. Polym.*, vol. 19, no. 1, Jan. 2022, doi: 10.1002/ppap.202100079.

[114] S. Meropoulis and C. A. Aggelopoulos, "Plasma microbubbles vs gas-liquid DBD energized by low-frequency high voltage nanopulses for pollutants degradation in water: Destruction mechanisms, composition of plasma-activated water and energy assessment," *J. Environ. Chem. Eng.*, vol. 11, no. 3, 2023, doi: 10.1016/j.jece.2023.109855.

[115] T.-H. Chung *et al.*, "Cell Electropermeabilisation Enhancement by Non-Thermal-Plasma-Treated PBS," *Cancers (Basel).*, vol. 12, no. 1, p. 219, Jan. 2020, doi: 10.3390/cancers12010219.

[116] R. Thirumdas *et al.*, "Plasma activated water (PAW): Chemistry, physico-chemical properties, applications in food and agriculture," *Trends Food Sci. Technol.*, vol. 77, no. March, pp. 21–31, Jul. 2018, doi: 10.1016/j.tifs.2018.05.007.

[117] A. da G. Sampaio, W. Chiappim, N. V. M. Milhan, B. Botan Neto, R. Pessoa, and C. Y. Koga-Ito, "Effect of the pH on the Antibacterial Potential and Cytotoxicity of Different Plasma-Activated Liquids," *Int. J. Mol. Sci.*, vol. 23, no. 22, p. 13893, Nov. 2022, doi: 10.3390/ijms232213893.

[118] S. Wu *et al.*, "Reactive radical-driven bacterial inactivation by hydrogen-peroxide-enhanced plasma-activated-water," *Eur. Phys. J. Spec. Top.*, vol. 226, no. 13, pp. 2887–2899, Aug. 2017, doi: 10.1140/epjst/e2016-60330-y.

[119] W. F. L. M. Hoeben, P. P. van Ooij, D. C. Schram, T. Huiskamp, A. J. M. Pemen, and P. Lukeš, "On the Possibilities of Straightforward Characterization of Plasma Activated Water," *Plasma Chem. Plasma Process.*, vol. 39, no. 3, pp. 597–626, May 2019, doi: 10.1007/s11090-019-09976-7.

[120] Y. Li, M. Hariharaputhiran, and S. V. Babu, "Chemical–mechanical polishing of copper and tantalum with silica abrasives," *J. Mater. Res.*, vol. 16, no. 4, pp. 1066–1073, Apr. 2001, doi: 10.1557/JMR.2001.0148.

[121] M. J. Peters, G. Stinstra, M. Hendriks, "Estimation of the Electrical Conductivity of Human Tissue," *Electromagnetics*, vol. 21, no. 7–8, pp. 545–557, Sep. 2001, doi: 10.1080/027263401752246199.

[122] Y. Zhao, S. Ojha, C. M. Burgess, D. Sun, and B. K. Tiwari, "Influence of various fish constituents on inactivation efficacy of plasma-activated water," *Int. J. Food Sci. Technol.*, vol. 55, no. 6, pp. 2630–2641, Jun. 2020, doi: 10.1111/ijfs.14516.

[123] D. Yan, N. Nourmohammadi, K. Bian, F. Murad, J. H. Sherman, and M. Keidar, "Stabilizing the cold plasma-stimulated medium by regulating medium's composition," *Sci. Rep.*, vol. 6, no. 1, p. 26016, May 2016, doi: 10.1038/srep26016.

[124] S. Mohades, N. Barekzi, H. Razavi, V. Maruthamuthu, and M. Laroussi, "Temporal evaluation of the anti-tumor efficiency of plasma-activated media," *Plasma Process. Polym.*, vol. 13, no. 12, pp. 1206–1211, Dec. 2016, doi: 10.1002/ppap.201600118.

[125] K. Kutasi and E. Tombácz, "Efficient trapping of RONS in gelatin and physiological solutions," *Plasma Process. Polym.*, vol. 19, no. 2, Feb. 2022, doi: 10.1002/ppap.202100077.

[126] P. Lukes, E. Dolezalova, I. Sisrova, and M. Clupek, "Aqueous-phase chemistry and bactericidal effects from an air discharge plasma in contact with water: evidence for the formation of peroxynitrite through a pseudo-second-order post-discharge reaction of H 2 O 2 and HNO 2," *Plasma Sources Sci. Technol.*, vol. 23, no. 1, p. 015019, Feb. 2014, doi: 10.1088/0963-0252/23/1/015019.

[127] E. Turrini *et al.*, "Plasma-activated medium as an innovative anticancer strategy: Insight into its cellular and molecular impact on in vitro leukemia cells," *Plasma Process. Polym.*, vol. 17, no. 10, pp. 1–14, Oct. 2020, doi: 10.1002/ppap.202000007.

[128] S. U. Kang *et al.*, "Nonthermal plasma induces head and neck cancer cell death: the potential involvement of mitogen-activated protein kinase-dependent mitochondrial reactive oxygen species," *Cell Death Dis.*, vol. 5, no. 2, pp. e1056–e1056, Feb. 2014, doi: 10.1038/cddis.2014.33.

[129] S. Kalghatgi *et al.*, "Effects of Non-Thermal Plasma on Mammalian Cells," *PLoS One*, vol. 6, no. 1, p. e16270, Jan. 2011, doi: 10.1371/journal.pone.0016270.

Supplementary Material

Investigation of the physicochemical properties and selective anti-cancer efficacy of in-plasma treated PBS using an exclusive liquid-submerged plasma jet

P. Shali[1,*$], N. Caz[2,*], J. Van den Bosch[2,*], R. Ghobeira[1], S. Aliakbarshirazi[1], M. Narimisa[1], R. Morent[1], E. Wolfs[2#], N. De Geyter[1#]

[1] *Research Unit Plasma Technology (RUPT), Department of Applied Physics, Faculty of Engineering and Architecture, Ghent University, Sint-Pietersnieuwstraat 41 B4, 9000 Ghent, Belgium*
[2] *Morphology Research Group, Biomedical Research Institute, Hasselt University, Campus Diepenbeek, Bioville, Diepenbeek, Belgium*

[*]Joint first authorship; [#]Joint last authorship
[$]Corresponding author,
e-mail address: parisa.shali@ugent.be

Supplementary Table 1. Positioning of the current paper in the available literature. Heatmap representing the inclusion of healthy cells as well as cancer cells, H_2O_2 and/or NO_2^- reconstituted controls and in liquid-submerged plasma reactors in papers involving the use of PTLs for cancer treatment. Papers are ranked according to 1) inclusion factor, 2) publication date, 3) alphabetical order of the first author name.

Authors (year)	Healthy versus cancer cells*	Reconstituted controls**	Plasma reactor configuration***	Ref.
Shali *et al.* (current paper)	1	3	1	
Kumar *et al.* (2016)	1	1	1	[1]
Poramapijitwat *et al.* (2023)	1	3	0	[2]
Pavlik *et al.* (2022)	1	3	0	[3]
Sklias *et al.* (2021)	1	3	0	[4]
Chen *et al.* (2017)	0	3	1	[5]
Girard *et al.* (2016)	1	3	0	[6]
Kurake *et al.* (2016)	1	3	0	[7]
Bisag *et al.* (2020)	1	2	0	[8]
Mateu-Sanz *et al.* (2020)	1	2	0	[9]
Miebach *et al.* (2022)	1	1▪	0	[10]
Turrini *et al.* (2020)	1	1	0	[11]
Freund *et al.* (2019)	1	1	0	[12]
Tornin *et al.* (2019)	1	1	0	[13]
Griseti *et al.* (2020)	0	3	0	[14]
Van Boxem *et al.* (2017)	0	3	0	[15]
Živanić *et al.* (2024)	0	1	0	[16]
Aguiar de Carvalho *et al.* (2022)	1	0	0	[17]
Sardella *et al.* (2021)	1	0	0	[18]
Terefinko *et al.* (2021)	1	0	0	[19]
Chung *et al.* (2020)	1	0	0	[20]
Nakamura *et al.* (2020)	1	0	0	[21]
Subramanian *et al.* (2020)	1	0	0	[22]
Xu *et al.* (2020)	1	0	0	[23]
Bauer *et al.* (2019)	1	0	0	[24]
Jezeh *et al.* (2019)	1	0	0	[25]
Chen *et al.* (2018)	1	0	0	[26]

Canal *et al.* (2017)	1	0	0	[27]
Nakamura *et al.* (2017)	1	0	0	[28]
Chen *et al.* (2016)	0	0	1	[29]
Hoan Nguyen *et al.* (2016)	1	0	0	[30]
Judée *et al.* (2016)	1	1	0	[31]
Mohades *et al.* (2016)	1	0	0	[32]
Tanaka *et al.* (2016)	1	0	0	[33]
Hattori *et al.* (2015)	1	0	0	[34]
Kumar *et al.* (2018)	0	1	0	[35]
Xu *et al.* (2018)	0	1	0	[36]
Judée *et al.* (2016)	0	1	0	[37]
Yokoyama *et al.* (2014)	0	1	0	[38]
Chaturvedi Misra *et al.* (2023)	0	0	0	[39]
Negi *et al.* (2023)	0	0	0	[40]
Xu *et al.* (2023)	0	0	0	[41]
Zhang *et al.* (2023)	0	0	0	[42]
Jo *et al.* (2022)	0	0	0	[43]
Li *et al.* (2022)	0	0	0	[44]
Zahedian *et al.* (2022)	0	0	0	[45]
Zhang *et al.* (2022)	0	0	0	[46]
Liu *et al.* (2021)	0	0	0	[47]
Zhang *et al.* (2021)	0	0	0	[48]
Zhang *et al.* (2021)	0	0	0	[49]
Hasse *et al.* (2020)	0	0	0	[50]
Yoshikawa *et al.* (2020)	0	0	0	[51]
Azzariti *et al.* (2019)	0	0	0	[52]
Bauer *et al.* (2019)	0	0	0	[53]
Chauvin *et al.* (2019)	0	0	0	[54]
Griseti *et al.* (2019)	0	0	0	[55]
Hoan Nguyen *et al.* (2018)	0	0	0	[56]
Privat-Maldonado *et al.* (2018)	0	0	0	[57]
Sato *et al.* (2018)	0	0	0	[58]
Chen *et al.* (2017)	0	0	0	[59]
Chen *et al.* (2017)	0	0	0	[60]
Takeda *et al.* (2017)	0	0	0	[61]
Adachi *et al.* (2015)	0	0	0	[62]
Hara *et al.* (2015)	0	0	0	[63]
Mohades *et al.* (2015)	0	0	0	[64]
Utsumi *et al.* (2013)	0	0	0	[65]
Vandamme *et al.* (2012)	0	0	0	[66]
Kim *et al.* (2010)	0	0	0	[67]

*0: only cancer cells; 1: cancer and healthy cells
**: 0: no control; 1: H_2O_2 control; 2: H_2O_2 and NO_2^- controls; 3: H_2O_2, NO_2^- and H_2O_2 + NO_2^- controls
***: 0: plasma reactor placed above the liquid to be treated; 1: in liquid-submerged plasma reactor

▪ Study comparing PTLs and reconstituted H_2O_2, $NO_3^-$and H_2O_2 + NO_3^- controls (no NO_2^- controls) *in vitro* and *in vivo* [10].

SUPPLEMENTARY MATERIALS AND METHODS

PBS temperature variation and liquid loss post-plasma treatment

The temperature of the PBS solutions was assessed using a portable digital thermometer (Pt500, Jumo, The Netherlands) before and immediately after plasma treatment. The temperature difference between these two time points was calculated to detect any heating effect induced by the plasma treatment. Given the fact that such heating effects may contribute, amongst other phenomena, to liquid evaporation, the plasma-induced liquid loss was also assessed. To do so, each liquid sample was weighed using a well-calibrated balance (Quintix224-1S, Sartorius GmbH, Germany) before and after treatment, and the mass difference was calculated. Based on the known density of 1x PBS, the volume of the evaporated PBS was calculated from the measured mass difference. All measurements were repeated 4 times across 4 independent plasma-treated PBS samples for each condition.

Electrical conductivity of PBS pre- and post-plasma treatment

The electrical conductivity of untreated and plasma-treated PBS were measured using a FiveEasy™ conductivity meter (Mettler Toledo, Switzerland). All measurements were done 4 times using 4 independently prepared plasma-treated samples for each condition.

SUPPLEMENTARY RESULTS AND DISCUSSION

Electrical characterization

Supplementary Figure 1 illustrates the V-I waveforms of the Ar APPJ generated at an applied voltage of 3.0 kV and a gas flow rate of 2.0 slm, supporting this choice. The waveforms display periodic plasma dynamics, with a sinusoidal voltage waveform and clear variations in the current waveform during each half cycle. Notably, intense current peaks occur due to a rapid increase in gas conductivity when the plasma ignites, followed by surface charge accumulation that reduces the gas voltage and terminates the discharge. Typically, the positive current pulse is slightly higher or equal in magnitude to the negative pulse. These distinct waveform profiles confirm that the discharge is operating in glow mode, characterized by stable, uniform plasma formation. In fact, periodic plasma dynamics with sinusoidal waveforms for the voltage are detected [68] [69] [70]. The waveforms obtained for the other plasma operational parameters used in this work are not included here as they strongly resemble the waveforms shown in Supplementary Figure 1.

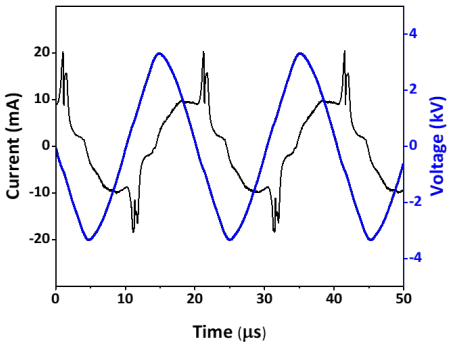

Supplementary Figure 1: Voltage and current waveforms recorded during the plasma treatment (gas flow rate: 2.0 slm, voltage: 3 kV).

Temperature and liquid loss

After characterizing the plasma itself, the subsequent experiments focused on how plasma exposure influences the temperature and liquid loss of the PBS solution. Initially, the PBS was set to room temperature (21°C) for all experiments, and the temperature was measured immediately following plasma exposure. Supplementary Figure 2 depicts the obtained changes in solution temperature as a function of voltage, flow rate and treatment time.

Supplementary Figure 2 (a) reveals that increasing the applied voltage leads to a slight rise in liquid temperature. At 2.0 kV, the temperature increases by 7.8 ± 0.6°C, which further rises to 9.9 ± 1.1°C at 3.5 kV. Statistical analysis using a T-test reveals a significant difference between these two values ($p \leq 0.05$). This can be explained as follows:

an increase in voltage is associated with a rise in discharge power, as illustrated in Figure 2 (a). This means that higher voltages thus enhance the conversion of electrical energy to plasma energy per unit of time. This more efficient energy transfer in turn results in an amplified temperature of the plasma-treated PBS, as the higher plasma energy can more effectively heat the surrounding medium. As shown in Supplementary Figure 2 (b), increasing the Ar flow rate from 1.0 to 2.5 slm slightly reduces the temperature increase from approximately 14°C to 10°C. This is consistent with prior studies, including the work of Hashim *et al.,* where a decrease in gas flow rate results in a higher plasma temperature [71]. The longer residence time of the gas within the plasma at lower flow rates allows it to absorb more energy, thus heating up the gas and as such the liquid [72]. Conversely, at higher flow rates, the plasma transfers less heat to the gas and liquid, leading to a smaller temperature increase.

Supplementary Figure 2 (c) illustrates that longer plasma exposure durations result in a continuous increase in liquid temperature, reaching 10.6°C after 10 minutes of plasma treatment. This increase is due to the steady transfer of energy from the plasma to the liquid over time. Upon plasma ignition, the energy present in the plasma heats the gas stream and this heat is then transferred to the treated liquid [73], causing a cumulative rise in the liquid temperature as the exposure time increases.

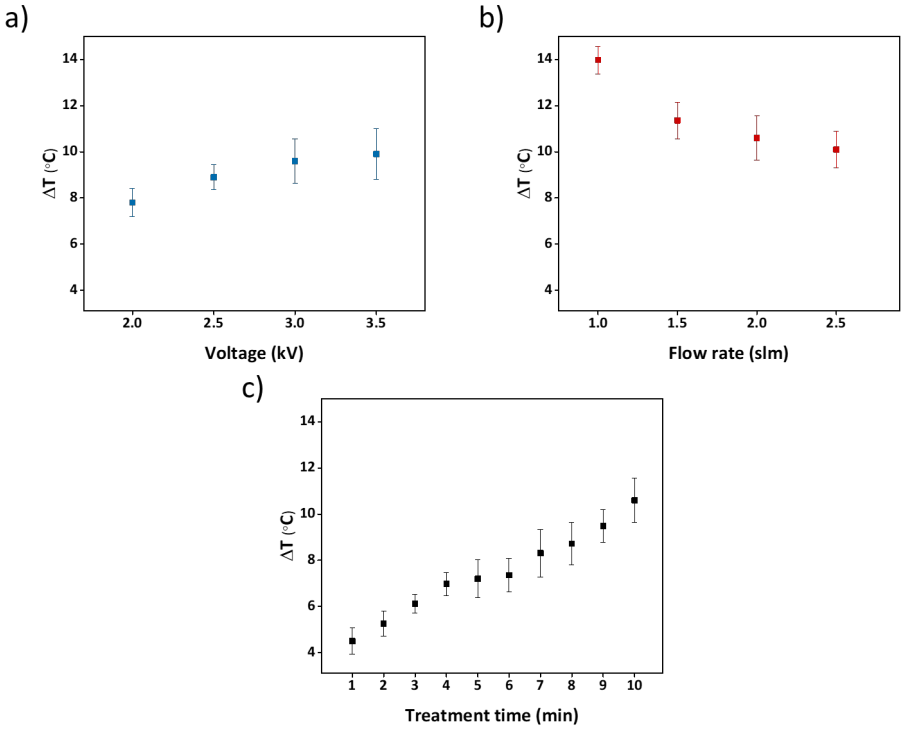

Supplementary Figure 2. Temperature difference ($\Delta T = T_{final} - T_{initial}$) upon plasma treatment of PBS for various (a) voltages, (b) flow rates, and (c) treatment times.

The liquid loss during the plasma treatment was also examined and the results are depicted in Supplementary Figure 3 as a function of voltage, flow rate and treatment time. As shown in Supplementary Figure 3 (a), increasing the voltage from 2.0 to 3.5 kV results in a 2.14-fold increase in the volume of PBS lost. Supplementary Figure 3 (b) reveals that an increase in the flow rate from 1.0 slm to 2.5 slm results in a 2.03-fold increase in the volume of PBS loss. On the other hand, Supplementary Figure 3 (c) shows that during the initial 3 minutes of plasma exposure, liquid loss remains minimal. However, starting from the 4th minute, liquid loss gradually increased, reaching 1.37 mL after a 10 minutes of treatment. When considering the liquid loss during plasma exposure, two factors should be taken into account: i) approximately 0.43 ± 0.1 mL of PBS adheres to the sample holder due to the submerged setup, making complete PBS collection after treatment impossible and ii) a portion of the liquid sample evaporates during plasma treatment. This evaporation has also been observed by Grande *et al.* when exposing a polycaprolactone solution in a mixture of chloroform and N,N-diformaldehyde to a similar submerged plasma jet [74]. Taking into account the volume of PBS adhering to the sample holder, it can be concluded that the liquid loss is minimal when using a plasma treatment time ≤ 3 min (voltage: 3 kV, flow rate: 2 slm), while it starts to become more pronounced at longer exposure times.

The data thus show that an increased voltage results in larger liquid volume loss, a finding which is consistent

with observations made by Li *et al.* [75]. Applying higher voltages results in the generation of a more energetic and intense plasma discharge. As demonstrated in Supplementary Figure 2 (a), this enhanced energy level results in the generation of more heat, causing the surrounding liquid to heat up and undergo evaporation more rapidly, which in turn increases the liquid loss. A similar explanation can be used to explain the influence of treatment time on the loss in PBS after plasma exposure, a finding that aligns with other research [76] [77] [78]. As treatment time progresses, the liquid heats up (Supplementary Figure 2 (c)), enhancing the rate of liquid evaporation and thus liquid loss. However, it is important to note that the evaporation rate is influenced not only by temperature but also by other factors such as surface area and the dynamics of the plasma-liquid interface, which may significantly impact liquid loss [79]. These factors can vary with changes in applied voltage and treatment duration, potentially contributing to the observed variations in liquid loss.

Other contributors than temperature are definitely in play when increasing the gas flow rate, as in this particular case the liquid temperature becomes smaller (Supplementary Figure 2 (b)), while the liquid loss increases. This larger liquid loss can be mainly attributed to differences in the plasma-liquid interface. Indeed, Rezaei *et al.* [68] have shown that an increase in gas flow rate strongly affects the plasma bubble dynamics inside the liquid, when using a similar submerged plasma jet. In fact, the bubble number density was found to considerably increase, resulting in more pronounced plasma-liquid interactions and thus a more efficient evaporation process. At higher gas flow rates, the energy of the plasma is very effectively transferred to the liquid molecules, allowing them to evaporate easily, thereby efficiently carrying away heat and diminishing the plasma-induced liquid heating, as shown in Supplementary Figure 2 (b).

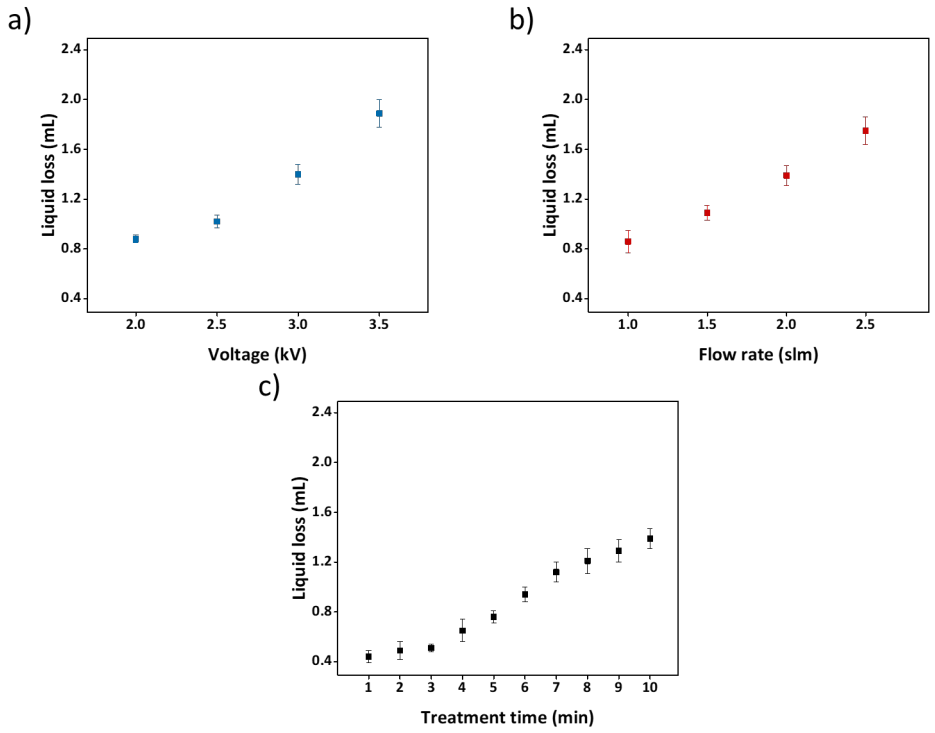

Supplementary Figure 3. Liquid loss during PBS plasma treatment as a function of (a) voltage, (b) flow rate, and (c) treatment time. Initial PBS volume: 5 mL.

In conclusion, the liquid loss in this work varies between 8.8% and 37.8%, depending on the used plasma operational parameters and considering the liquid adhering to the sample holder. Comparatively, studies using above-liquid plasma configurations with PBS have reported varying rates of liquid loss, such as 100% loss after a 5 minute treatment [76], 20% loss after a 10 minute treatment [78], and 15.6% loss after a 30 minute treatment [80]. The evaporation rates found in this study are within or below these previously reported values, suggesting that the submerged plasma set-up used in this study offers a comparable or better efficiency in minimizing liquid loss during plasma treatment.

REFERENCES

[1] N. Kumar, J. H. Park, S. N. Jeon, B. S. Park, E. H. Choi, and P. Attri, "The action of microsecond-pulsed plasma-activated media on the inactivation of human lung cancer cells," *J. Phys. D. Appl. Phys.*, vol. 49, no. 11, p. 115401, Mar. 2016, doi: 10.1088/0022-3727/49/11/115401.

[2] P. Poramapijitwat, P. Thana, P. Sukum, Y. Liangdeng, C. Kuensaen, and D. Boonyawan, "Selective Cytotoxicity of Lung Cancer Cells—A549 and H1299—Induced by Ringer's Lactate Solution Activated by a Non-thermal Air Plasma Jet Device, Nightingale®," *Plasma Chem. Plasma Process.*, vol. 43, no. 4, pp. 805–830, Jul. 2023, doi: 10.1007/s11090-023-10330-1.

[3] T. I. Pavlik, N. G. Gusein-zade, L. V. Kolik, and N. L. Shimanovskii, "Comparison of the Biological Properties of Plasma-Treated Solution and Solution of Chemical Reagents," *Appl. Sci.*, vol. 12, no. 8, p. 3704, Apr. 2022, doi: 10.3390/app12083704.

[4] K. Sklias, J. S. Sousa, and P. M. Girard, "Role of short- and long-lived reactive species on the selectivity and anti-cancer action of plasma treatment in vitro," *Cancers (Basel).*, vol. 13, no. 4, pp. 1–31, 2021, doi: 10.3390/cancers13040615.

[5] Z. Chen, X. Cheng, L. Lin, and M. Keidar, "Cold atmospheric plasma discharged in water and its potential use in cancer therapy," *J. Phys. D. Appl. Phys.*, vol. 50, no. 1, p. 015208, Jan. 2017, doi: 10.1088/1361-6463/50/1/015208.

[6] P.-M. Girard *et al.*, "Synergistic Effect of H2O2 and NO2 in Cell Death Induced by Cold Atmospheric He Plasma," *Sci. Rep.*, vol. 6, no. 1, p. 29098, Jul. 2016, doi: 10.1038/srep29098.

[7] N. Kurake *et al.*, "Cell survival of glioblastoma grown in medium containing hydrogen peroxide and/or nitrite, or in plasma-activated medium," *Arch. Biochem. Biophys.*, vol. 605, pp. 102–108, Sep. 2016, doi: 10.1016/j.abb.2016.01.011.

[8] A. Bisag *et al.*, "Plasma-activated ringer's lactate solution displays a selective cytotoxic effect on ovarian cancer cells," *Cancers (Basel).*, vol. 12, no. 2, pp. 1–15, 2020, doi: 10.3390/cancers12020476.

[9] M. Mateu-Sanz *et al.*, "Cold Plasma-Treated Ringer's Saline: A Weapon to Target Osteosarcoma," *Cancers (Basel).*, vol. 12, no. 1, p. 227, Jan. 2020, doi: 10.3390/cancers12010227.

[10] L. Miebach, E. Freund, R. Clemen, S. Kersting, L.-I. Partecke, and S. Bekeschus, "Gas plasma–oxidized sodium chloride acts via hydrogen peroxide in a model of peritoneal carcinomatosis," *Proc. Natl. Acad. Sci.*, vol. 119, no. 31, Aug. 2022, doi: 10.1073/pnas.2200708119.

[11] E. Turrini *et al.*, "Plasma-activated medium as an innovative anticancer strategy: Insight into its cellular and molecular impact on in vitro leukemia cells," *Plasma Process. Polym.*, vol. 17, no. 10, pp. 1–14, Oct. 2020, doi: 10.1002/ppap.202000007.

[12] E. Freund *et al.*, "Physical plasma-treated saline promotes an immunogenic phenotype in CT26 colon cancer cells in vitro and in vivo," *Sci. Rep.*, vol. 9, no. 1, p. 634, Jan. 2019, doi: 10.1038/s41598-018-37169-3.

[13] J. Tornin, M. Mateu-Sanz, A. Rodríguez, C. Labay, R. Rodríguez, and C. Canal, "Pyruvate Plays a Main Role in the Antitumoral Selectivity of Cold Atmospheric Plasma in Osteosarcoma," *Sci. Rep.*, vol. 9, no. 1, p. 10681, Jul. 2019, doi: 10.1038/s41598-019-47128-1.

[14] E. Griseti, N. Merbahi, and M. Golzio, "Anti-cancer potential of two plasma-activated liquids: Implication of long-lived reactive oxygen and nitrogen species," *Cancers (Basel).*, vol. 12, no. 3, 2020, doi: 10.3390/cancers12030721.

[15] W. Van Boxem *et al.*, "Anti-cancer capacity of plasma-treated PBS: effect of chemical composition on cancer cell cytotoxicity," *Sci. Rep.*, vol. 7, no. 1, p. 16478, Nov. 2017, doi: 10.1038/s41598-017-16758-8.

[16] M. Živanić *et al.*, "Injectable Plasma-Treated Alginate Hydrogel for Oxidative Stress Delivery to Induce Immunogenic Cell Death in Osteosarcoma," *Adv. Funct. Mater.*, vol. 34, no. 14, Apr. 2024, doi: 10.1002/adfm.202312005.

[17] A. M. Aguiar de Carvalho, L. Scally, B. Tiwari, P. J. Cullen, and J. F. Curtin, "Synergistic cytotoxicity from cold atmospheric plasma and ultrasound in glioma cells," *Plasma Process. Polym.*, vol. 19, no. 8, Aug. 2022, doi: 10.1002/ppap.202200042.

[18] E. Sardella *et al.*, "Plasma Treated Water Solutions in Cancer Treatments: The Contrasting Role of RNS," *Antioxidants*, vol. 10, no. 4, p. 605, Apr. 2021, doi: 10.3390/antiox10040605.

[19] D. Terefinko, A. Dzimitrowicz, A. Bielawska-Pohl, A. Klimczak, P. Pohl, and P. Jamroz, "The Influence of Cold Atmospheric Pressure Plasma-Treated Media on the Cell Viability, Motility, and Induction of Apoptosis in Human Non-Metastatic (MCF7) and Metastatic (MDA-MB-231) Breast Cancer Cell Lines," *Int. J. Mol. Sci.*, vol. 22, no. 8, p. 3855, Apr. 2021, doi: 10.3390/ijms22083855.

[20] T.-H. Chung *et al.*, "Cell Electropermeabilisation Enhancement by Non-Thermal-Plasma-Treated PBS," *Cancers (Basel).*, vol. 12, no. 1, p. 219, Jan. 2020, doi: 10.3390/cancers12010219.

[21] K. Nakamura *et al.*, "Preclinical Verification of the Efficacy and Safety of Aqueous Plasma for Ovarian Cancer Therapy," *Cancers (Basel).*, vol. 13, no. 5, p. 1141, Mar. 2021, doi: 10.3390/cancers13051141.

[22] P. S. G. Subramanian, A. Jain, A. M. Shivapuji, N. R. Sundaresan, S. Dasappa, and L. Rao, "Plasma-activated water from a dielectric barrier discharge plasma source for the selective treatment of cancer cells," *Plasma Process. Polym.*, vol. 17, no. 8, pp. 1–13, Aug. 2020, doi: 10.1002/ppap.201900260.

[23] S. Xu *et al.*, "Cold atmospheric plasma-activated Ringer's solution inhibits the proliferation of osteosarcoma cells through the mitochondrial apoptosis pathway," *Oncol. Rep.*, vol. 43, no. 5, pp. 1683–1691, Feb. 2020, doi: 10.3892/or.2020.7518.

[24] G. Bauer, D. Sersenová, D. B. Graves, and Z. Machala, "Cold Atmospheric Plasma and Plasma-Activated Medium Trigger RONS-Based Tumor Cell Apoptosis," *Sci. Rep.*, vol. 9, no. 1, p. 14210, Oct. 2019, doi: 10.1038/s41598-019-50291-0.

[25] M. A. Jezeh, T. Tayebi, M. R. Khani, H. Niknejad, and B. Shokri, "Direct cold atmospheric plasma and plasma-activated medium effects on breast and cervix cancer cells," *Plasma Process. Polym.*, vol. 17, no. 11, pp. 1–14, Nov. 2020, doi: 10.1002/ppap.201900241.

[26] Z. Chen, L. Lin, E. Gjika, X. Cheng, J. Canady, and M. Keidar, "Selective Treatment of Pancreatic Cancer Cells by Plasma-Activated Saline Solutions," *IEEE Trans. Radiat. Plasma Med. Sci.*, vol. 2, no. 2, pp. 116–120, Mar. 2018, doi: 10.1109/TRPMS.2017.2761192.

[27] C. Canal, R. Fontelo, I. Hamouda, J. Guillem-Marti, U. Cvelbar, and M.-P. Ginebra, "Plasma-induced selectivity in bone cancer cells death," *Free Radic. Biol. Med.*, vol. 110, no. May, pp. 72–80, Sep. 2017, doi: 10.1016/j.freeradbiomed.2017.05.023.

[28] K. Nakamura *et al.*, "Novel Intraperitoneal Treatment With Non-Thermal Plasma-Activated Medium Inhibits Metastatic Potential of Ovarian Cancer Cells," *Sci. Rep.*, vol. 7, no. 1, p. 6085, Jul. 2017, doi: 10.1038/s41598-017-05620-6.

[29] Z. Chen, L. Lin, X. Cheng, E. Gjika, and M. Keidar, "Effects of cold atmospheric plasma generated in deionized water in cell cancer therapy," *Plasma Process. Polym.*, vol. 13, no. 12, pp. 1151–1156, Dec. 2016, doi: 10.1002/ppap.201600086.

[30] N. H. Nguyen, H. J. Park, S. S. Yang, K. S. Choi, and J.-S. Lee, "Anti-cancer efficacy of nonthermal plasma dissolved in a liquid, liquid plasma in heterogeneous cancer cells," *Sci. Rep.*, vol. 6, no. 1, p. 29020, Jul. 2016, doi: 10.1038/srep29020.

[31] J. Florian, N. Merbahi, and M. Yousfi, "Genotoxic and Cytotoxic Effects of Plasma-Activated Media on Multicellular Tumor Spheroids," *Plasma Med.*, vol. 6, no. 1, pp. 47–57, 2016, doi: 10.1615/PlasmaMed.2016015823.

[32] S. Mohades, N. Barekzi, H. Razavi, V. Maruthamuthu, and M. Laroussi, "Temporal evaluation of the anti-tumor efficiency of plasma-activated media," *Plasma Process. Polym.*, vol. 13, no. 12, pp. 1206–1211, Dec. 2016, doi: 10.1002/ppap.201600118.

[33] H. Tanaka *et al.*, "Non-thermal atmospheric pressure plasma activates lactate in Ringer's solution for anti-tumor effects," *Sci. Rep.*, vol. 6, no. 1, p. 36282, Nov. 2016, doi: 10.1038/srep36282.

[34] N. HATTORI *et al.*, "Effectiveness of plasma treatment on pancreatic cancer cells," *Int. J. Oncol.*, vol. 47, no. 5, pp. 1655–1662, Nov. 2015, doi: 10.3892/ijo.2015.3149.

[35] N. Kumar, P. Attri, S. Dewilde, and A. Bogaerts, "Inactivation of human pancreatic ductal adenocarcinoma with atmospheric plasma treated media and water: a comparative study," *J. Phys. D. Appl. Phys.*, vol. 51, no. 25, p. 255401, Jun. 2018, doi: 10.1088/1361-6463/aac571.

[36] D. Xu *et al.*, "NO2- and NO3- enhance cold atmospheric plasma induced cancer cell death by generation of ONOO-," *AIP Adv.*, vol. 8, no. 10, Oct. 2018, doi: 10.1063/1.5046353.

[37] F. Judée, C. Fongia, B. Ducommun, M. Yousfi, V. Lobjois, and N. Merbahi, "Short and long time effects of low temperature Plasma Activated Media on 3D multicellular tumor spheroids," *Sci. Rep.*, vol. 6, no. 1, p. 21421, Feb. 2016, doi: 10.1038/srep21421.

[38] M. Yokoyama, K. Johkura, and T. Sato, "Gene expression responses of HeLa cells to chemical species generated by an atmospheric plasma flow," *Biochem. Biophys. Res. Commun.*, vol. 450, no. 4, pp. 1266–1271, Aug. 2014, doi: 10.1016/j.bbrc.2014.06.116.

[39] V. Chaturvedi Misra, G. Pai B, N. Tiwari, B. S. Patro, and S. Ghorui, "Excitation Frequency Effect on Breast Cancer Cell Death by Atmospheric Pressure Cold Plasma," *Plasma Chem. Plasma Process.*, vol. 43, no. 2, pp. 467–490, Mar. 2023, doi: 10.1007/s11090-023-10312-3.

[40] M. Negi, N. Kaushik, L. N. Nguyen, E. H. Choi, and N. K. Kaushik, "Argon gas plasma-treated physiological solutions stimulate immunogenic cell death and eradicates immunosuppressive CD47 protein in lung carcinoma," *Free Radic. Biol. Med.*, vol. 201, no. March, pp. 26–40, May 2023, doi: 10.1016/j.freeradbiomed.2023.03.009.

[41] H. Xu *et al.*, "Enhancement of the drug sensitization of cancer cells by plasma-activated saline," *Plasma Process. Polym.*, vol. 20, no. 9, pp. 1–9, Sep. 2023, doi: 10.1002/ppap.202300001.

[42] J. Zhang *et al.*, "Study on the Anticancer Effects of Plasma-Activated Saline Perfusion Based on a Microfluidic System," *Plasma Chem. Plasma Process.*, vol. 43, no. 1, pp. 99–110, Jan. 2023, doi: 10.1007/s11090-022-10297-5.

[43] A. Jo *et al.*, "Plasma-activated medium induces ferroptosis by depleting FSP1 in human lung cancer cells," *Cell Death Dis.*, vol. 13, no. 3, p. 212, Mar. 2022, doi: 10.1038/s41419-022-04660-9.

[44] Y. Li *et al.*, "Low-Temperature Plasma-Activated Medium Inhibited Proliferation and Progression of Lung Cancer by Targeting the PI3K/Akt and MAPK Pathways," *Oxid. Med. Cell. Longev.*, vol. 2022, pp. 1–18, Mar. 2022, doi: 10.1155/2022/9014501.

[45] S. Zahedian, A. Hekmat, S. Hesami Tackallou, and M. Ghoranneviss, "The Impacts of Prepared Plasma-Activated Medium (PAM) Combined with Doxorubicin on the Viability of MCF-7 Breast Cancer Cells: A New Cancer Treatment Strategy," *Reports Biochem. Mol. Biol.*, vol. 10, no. 4, pp. 640–652, Jan. 2022, doi: 10.52547/rbmb.10.4.640.

[46] J. Zhang *et al.*, "Investigation of different solutions activated by air plasma jet and their anticancer effect," *Appl. Phys. Lett.*, vol. 120, no. 26, Jun. 2022, doi: 10.1063/5.0096605.

[47] Z. Liu *et al.*, "The impact of surface-to-volume ratio on the plasma activated water characteristics and its anticancer effect," *J. Phys. D. Appl. Phys.*, vol. 54, no. 21, p. 215203, May 2021, doi: 10.1088/1361-6463/abe78f.

[48] H. Zhang *et al.*, "Antitumor effects of hyperthermia with plasma-treated solutions on 3D bladder tumor spheroids," *Plasma Process. Polym.*, vol. 18, no. 10, pp. 1–8, Oct. 2021, doi: 10.1002/ppap.202100070.

[49] H. Zhang, J. Zhang, B. Guo, H. Chen, D. Xu, and M. G. Kong, "The Antitumor Effects of Plasma-Activated Saline on Muscle-Invasive Bladder Cancer Cells In Vitro and In Vivo Demonstrate Its Feasibility as a Potential Therapeutic Approach," *Cancers (Basel).*, vol. 13, no. 5, p. 1042, Mar. 2021, doi: 10.3390/cancers13051042.

[50] S. Hasse, T. Meder, E. Freund, T. von Woedtke, and S. Bekeschus, "Plasma Treatment Limits Human Melanoma Spheroid Growth and Metastasis Independent of the Ambient Gas Composition," *Cancers (Basel).*, vol. 12, no. 9, p. 2570, Sep. 2020, doi: 10.3390/cancers12092570.

[51] N. Yoshikawa *et al.*, "Plasma-activated medium promotes autophagic cell death along with alteration of the mTOR pathway," *Sci. Rep.*, vol. 10, no. 1, p. 1614, Jan. 2020, doi: 10.1038/s41598-020-58667-3.

[52] A. Azzariti *et al.*, "Plasma-activated medium triggers cell death and the presentation of immune activating danger signals in melanoma and pancreatic cancer cells," *Sci. Rep.*, vol. 9, no. 1, pp. 1–13, 2019, doi: 10.1038/s41598-019-40637-z.

[53] G. Bauer, D. Sersenová, D. B. Graves, and Z. Machala, "Dynamics of Singlet Oxygen-Triggered, RONS-Based Apoptosis Induction after Treatment of Tumor Cells with Cold Atmospheric Plasma or Plasma-Activated Medium," *Sci. Rep.*, vol. 9, no. 1, p. 13931, Sep. 2019, doi: 10.1038/s41598-019-50329-3.

[54] J. Chauvin *et al.*, "Elucidation of in vitro cellular steps induced by antitumor treatment with plasma-activated medium," *Sci. Rep.*, vol. 9, no. 1, p. 4866, Mar. 2019, doi: 10.1038/s41598-019-41408-6.

[55] E. Griseti *et al.*, "Pulsed Electric Field Treatment Enhances the Cytotoxicity of Plasma-Activated Liquids in a Three-Dimensional Human Colorectal Cancer Cell Model," *Sci. Rep.*, vol. 9, no. 1, p. 7583, May 2019, doi: 10.1038/s41598-019-44087-5.

[56] N. Nguyen, H. Park, S. Hwang, J.-S. Lee, and S. Yang, "Anticancer Efficacy of Long-Term Stored Plasma-Activated Medium," *Appl. Sci.*, vol. 9, no. 4, p. 801, Feb. 2019, doi: 10.3390/app9040801.

[57] A. Privat-Maldonado, Y. Gorbanev, S. Dewilde, E. Smits, and A. Bogaerts, "Reduction of Human Glioblastoma Spheroids Using Cold Atmospheric Plasma: The Combined Effect of Short- and Long-Lived Reactive Species," *Cancers (Basel).*, vol. 10, no. 11, p. 394, Oct. 2018, doi: 10.3390/cancers10110394.

[58] Y. Sato *et al.*, "Effect of Plasma-Activated Lactated Ringer's Solution on Pancreatic Cancer Cells In Vitro and In Vivo," *Ann. Surg. Oncol.*, vol. 25, no. 1, pp. 299–307, Jan. 2018, doi: 10.1245/s10434-017-6239-y.

[59] Z. Chen *et al.*, "A Novel Micro Cold Atmospheric Plasma Device for Glioblastoma Both In Vitro and In Vivo," *Cancers (Basel).*, vol. 9, no. 12, p. 61, May 2017, doi: 10.3390/cancers9060061.

[60] Z. Chen, S. Zhang, I. Levchenko, I. I. Beilis, and M. Keidar, "In vitro Demonstration of Cancer Inhibiting Properties from Stratified Self-Organized Plasma-Liquid Interface," *Sci. Rep.*, vol. 7, no. 1, p. 12163, Sep. 2017, doi: 10.1038/s41598-017-12454-9.

[61] S. Takeda *et al.*, "Intraperitoneal Administration of Plasma-Activated Medium: Proposal of a Novel Treatment Option for Peritoneal Metastasis From Gastric Cancer," *Ann. Surg. Oncol.*, vol. 24, no. 5, pp. 1188–1194, May 2017, doi: 10.1245/s10434-016-5759-1.

[62] T. Adachi, H. Tanaka, S. Nonomura, H. Hara, S. Kondo, and M. Hori, "Plasma-activated medium induces A549 cell injury via a spiral apoptotic cascade involving the mitochondrial–nuclear network," *Free Radic. Biol. Med.*, vol. 79, pp. 28–44, Feb. 2015, doi: 10.1016/j.freeradbiomed.2014.11.014.

[63] H. Hara, M. Taniguchi, M. Kobayashi, T. Kamiya, and T. Adachi, "Plasma-activated medium-induced intracellular zinc liberation causes death of SH-SY5Y cells," *Arch. Biochem. Biophys.*, vol. 584, pp. 51–60, Oct. 2015, doi: 10.1016/j.abb.2015.08.014.

[64] S. Mohades, M. Laroussi, J. Sears, N. Barekzi, and H. Razavi, "Evaluation of the effects of a plasma activated medium on cancer

cells," *Phys. Plasmas*, vol. 22, no. 12, Dec. 2015, doi: 10.1063/1.4933367.
[65] F. Utsumi *et al.*, "Effect of Indirect Nonequilibrium Atmospheric Pressure Plasma on Anti-Proliferative Activity against Chronic Chemo-Resistant Ovarian Cancer Cells In Vitro and In Vivo," *PLoS One*, vol. 8, no. 12, p. e81576, Dec. 2013, doi: 10.1371/journal.pone.0081576.
[66] M. Vandamme *et al.*, "ROS implication in a new antitumor strategy based on non-thermal plasma," *Int. J. Cancer*, vol. 130, no. 9, pp. 2185–2194, May 2012, doi: 10.1002/ijc.26252.
[67] C.-H. Kim *et al.*, "Induction of cell growth arrest by atmospheric non-thermal plasma in colorectal cancer cells," *J. Biotechnol.*, vol. 150, no. 4, pp. 530–538, Dec. 2010, doi: 10.1016/j.jbiotec.2010.10.003.
[68] F. Rezaei, A. Nikiforov, R. Morent, and N. De Geyter, "Plasma Modification of Poly Lactic Acid Solutions to Generate High Quality Electrospun PLA Nanofibers," *Sci. Rep.*, vol. 8, no. 1, p. 2241, Feb. 2018, doi: 10.1038/s41598-018-20714-5.
[69] J. L. Walsh, F. Iza, N. B. Janson, V. J. Law, and M. G. Kong, "Three distinct modes in a cold atmospheric pressure plasma jet," *J. Phys. D. Appl. Phys.*, vol. 43, no. 7, 2010, doi: 10.1088/0022-3727/43/7/075201.
[70] J. P. Boeuf, "Plasma display panels: Physics, recent developments and key issues," *J. Phys. D. Appl. Phys.*, vol. 36, no. 6, 2003, doi: 10.1088/0022-3727/36/6/201.
[71] K. A. Aadim, "Effect of gas flow rate on plasma temperature and electron density of atmospheric argon plasma jet," *Iraqi J. Phys.*, vol. 15, no. 35, pp. 117–124, Oct. 2018, doi: 10.30723/ijp.v15i35.60.
[72] M. Ramakers, G. Trenchev, S. Heijkers, W. Wang, and A. Bogaerts, "Gliding Arc Plasmatron: Providing an Alternative Method for Carbon Dioxide Conversion," *ChemSusChem*, vol. 10, no. 12, pp. 2642–2652, 2017, doi: 10.1002/cssc.201700589.
[73] J. Qian, W. Yan, W. Zhang, J. Zhang, J. Wang, and V. Raghavan, "Plasma-activated water: Perspective of the theoretical model, safety assessment and application in animal-derived products," *Trends Food Sci. Technol.*, vol. 143, no. December 2023, p. 104282, Jan. 2024, doi: 10.1016/j.tifs.2023.104282.
[74] S. Grande *et al.*, "Atmospheric Pressure Plasma Jet Treatment of Poly-ε-caprolactone Polymer Solutions To Improve Electrospinning," *ACS Appl. Mater. Interfaces*, vol. 9, no. 38, pp. 33080–33090, Sep. 2017, doi: 10.1021/acsami.7b08439.
[75] Y. Li, Z. Song, T. Zhang, W. Xu, C. Ding, and H. Chen, "Spectral Characteristics of Needle Array-Plate Dielectric Barrier Discharge Plasma and Its Activated Water," *J. Spectrosc.*, vol. 2021, pp. 1–13, Nov. 2021, doi: 10.1155/2021/9771245.
[76] K. Pansare *et al.*, "Effect of Cold Atmospheric Plasma Jet and Gamma Radiation Treatments on Gingivobuccal Squamous Cell Carcinoma and Breast Adenocarcinoma Cells," *Plasma Chem. Plasma Process.*, vol. 42, no. 1, pp. 163–178, Jan. 2022, doi: 10.1007/s11090-021-10212-4.
[77] A. da G. Sampaio, W. Chiappim, N. V. M. Milhan, B. Botan Neto, R. Pessoa, and C. Y. Koga-Ito, "Effect of the pH on the Antibacterial Potential and Cytotoxicity of Different Plasma-Activated Liquids," *Int. J. Mol. Sci.*, vol. 23, no. 22, p. 13893, Nov. 2022, doi: 10.3390/ijms232213893.
[78] F. Girard *et al.*, "Formation of reactive nitrogen species including peroxynitrite in physiological buffer exposed to cold atmospheric plasma," *RSC Adv.*, vol. 6, no. 82, pp. 78457–78467, 2016, doi: 10.1039/C6RA12791F.
[79] A. Khlyustova and A. Maksimov, "Double Electrical Layer at the Plasma-Solution Interface," *Contrib. to Plasma Phys.*, vol. 53, no. 6, pp. 481–491, Jun. 2013, doi: 10.1002/ctpp.201200105.
[80] P. Svarnas *et al.*, "Water Modification by Cold Plasma Jet with Respect to Physical and Chemical Properties," *Appl. Sci.*, vol. 12, no. 23, p. 11950, Nov. 2022, doi: 10.3390/app122311950.